ABSTRACT

SUBMICRON PATTERNING USING LASER INTERFERENCE LITHOGRAPHY

by
Luigi Pollara Verdoni

In this thesis, the theory, fabrication protocol, and initial results of an alternative nano-patterning technique called Interferometric Lithography (IL) are presented. Comprised of the identical process attributes of traditional projection photolithography, IL mirrors the wafer preparation and development procedures of our existing clean room capabilities. The main departure is solely in means of pattern delineation. IL is a "mask less" technique that employs the interference fringe pattern of two coherent beams, and can therefore be generated with a commercial laser. Due to its simplicity, Interferometric Lithography provides an attractive supplement to existing methods of nano-patterning.

Utilizing a 325 nm HeCd laser and a wavefront division interferometer, a grating with a period resolution of 600 nm was achieved. An effective protocol was evaluated for quantifying the exposure characteristics of Shipley 1805 positive photoresist. In addition, an optical diagnostic was developed to interrogate the integrity of the grating structure, providing a qualitative assessment prior to investigation under the electron microscope.

SUBMICRON PATTERNING USING LASER INTERFERENCE LITHOGRAPHY

by
Luigi Pollara Verdoni

A Thesis
Submitted to the Faculty of
New Jersey Institute of Technology
in Partial Fulfillment of the Requirements for the Degree of
Master of Science in Materials Science & Engineering

Department of Materials Science & Engineering

August 2006

APPROVAL PAGE

SUBMICRON PATTERNING USING LASER INTERFERENCE LITHOGRAPHY

Luigi Pollara Verdoni

06/14/06

Dr. Leonid Tsybeskov, Thesis Advisor — Date
Associate Professor of Electrical and Computer Engineering, NJIT

06/14/2006

Dr. Dentcho Ivanov, Committee Member — Date
Director Microelectronics Fabrication Center, NJIT

06/14/2006

Dr. Andrei Sirenko, Committee Member — Date
Assistant Professor of Applied Physics, NJIT

BIOGRAPHICAL SKETCH

Author: Luigi Pollara Verdoni

Degree: Master of Science

Date: August 2006

Undergraduate and Graduate Education:

- Master of Science in Materials Science & Engineering,
  New Jersey Institute of Technology, Newark, NJ, 2006

- Bachelor of Science in Optics,
  University of Rochester, Rochester, NY, 2000

Major: Materials Science & Engineering

This thesis is dedicated to my beloved family, John, Marietta, Angelo, and Rose, and to the memory of my dog, Lila.

ACKNOWLEDGMENT

The author would like to express his deep gratitude to his advisor, Dr. Leonid Tsybeskov, for the guidance, inspiration, and support throughout this research project and thesis.

Special thanks are given to Dr. Dentcho Ivanov and Dr. Andrei Sirenko, the members of this committee, for taking the time to review this thesis and actively participating in this committee. In addition, this research benefited greatly from the support of the Office of Research and Development.

TABLE OF CONTENTS

LIST OF FIGURES

CHAPTER 1

INTRODUCTION

1.1 Research Motivation and Scope

The insatiable consumer demand for sophisticated computing applications has led to the widespread proliferation of digital media. Advances in processing, data storage, and internet communications have necessitated the rapid evolution of the contemporary microprocessor. The vast strides in processor performance speeds can be proportionally linked to the progress in reducing the size of the microprocessor. Advancement over the previous four decades has led to the reduction of feature sizes by a factor of two virtually every 18 months [1].

The semiconductor industry has met this challenge and is poised to attain 45-nm features by 2010. However, future progression for device miniaturization will push conventional patterning techniques to their theoretical limits and require the employment of complementary fabrication methods. Modern nanotechnologists continue to draw upon theories and practices from both traditional solid state physics and more recent chemical and bio-inspired arenas. This departure from the standard demarcation between traditional VLSI (Very Large Scale Integration), and "Wet" chemical techniques is most evident in the field of nanopatterning, where the merging of "Top-Down" [2-5] and "Bottom-up" [6-8] paradigms have literally allowed the fabrication of custom materials one molecule at a time. Though largely motivated by the semiconductor industry, the techniques employed for obtaining nanometer digital device structures have facilitated substantial breakthroughs in multiple disciplines. VLSI patterning methods have become invaluable to a broad

spectrum of technologies including, field emission displays [9], nanofluidic devices [10], block copolymers [11], and template induced growth of nano-structures [12]. Advancements in the conventional photolithographic system continue to form the infrastructure for high resolution nanopatterning, enabling extensive progress in a variety of applications beyond semiconductor electronics.

1.2 Conventional Photolithography

The inception of the integrated circuit was a seminal event that heralded not only the dawn of computers, but the standard manufacturing processes that have culminated to what we refer to today as VLSI or very-large-scale-integration. This term denotes electronic chips with 10^5-10^6 transistors on the board. VLSI primarily employs the standard device fabrication and integration technique of Photolithography (Figure 1.1). A semiconductor wafer is decontaminated and placed in an oven where a protective oxide layer is grown, this layer is integral to future device architecture, and aids in the demarcation of subsequent patterning. A photo-sensitive polymer, or photoresist containing photoinitiators, photosensitive resin, and additives, are applied via spin coating. An intermediary heat treatment ensures the uniformity and integrity of the layer upon the oxide/wafer stack, and the removal of excess solvent. The desired mask pattern, containing the intricate board layout, is transferred to the resist coated wafer through sufficient exposure to optical radiation. The photosensitive resin can be either polymerized/crosslinked, or decomposed via the generation of radicals or cations. This results in a solubility change from the initial medium. Subsequent chemical development effectively removes the soluble areas of the

desired pattern and the resultant structure is rendered. Final testing and packaging is performed and the electronic device is ready for further integration.

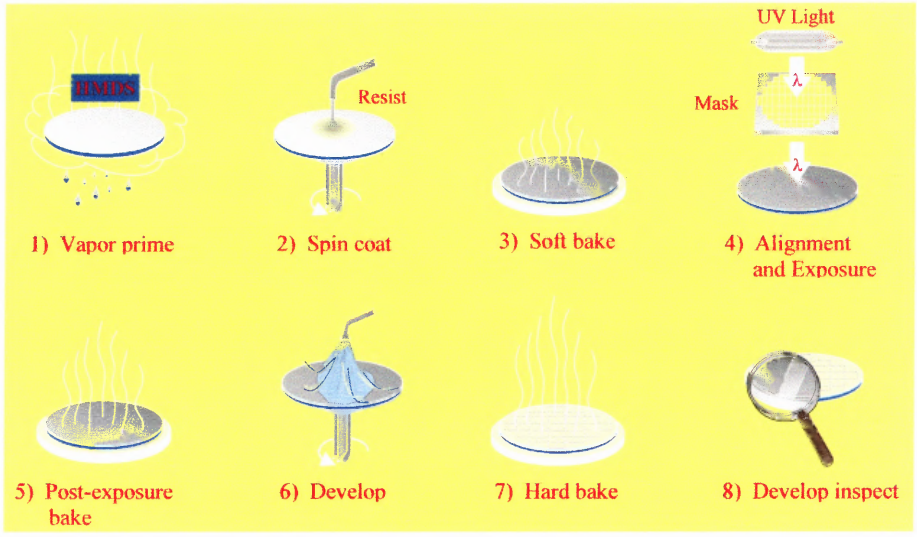

Figure 1.1 Conventional semiconductor fabrication processes.

The semiconductor industry continues to rely on projection photolithography as the patterning foundation for the fabrication of electronic devices [13]. Comprised of three main components, the standard projection photolithographic system (Figure 1.2) consists of a high powered light source and delivery optics, or condenser lens, for illumination. The second component consists of an intricate photo-mask possessing the layout of the integrated circuit. The final component is the optical projection lens, whose utility is for final imprinting of feature on wafer. The critical dimension or minimum feature that can be printed is governed by the Rayleigh equation for resolution given in Equation 1.1.

$$R = k_1 \lambda / \mathrm{NA} \tag{1.1}$$

Where R is the resolution, or minimum feature size, λ is the wavelength of exposing radiation, NA is the numerical aperture of the projection optical system, and k_1 is the

resolution parameter that encapsulates the variables of the photolithographic process such as resist quality, thermal bakes and resolution enhancement techniques.

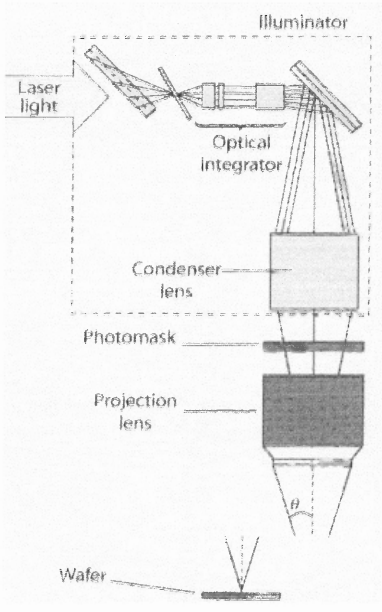

Figure 1.2 Contemporary system for projection photolithography [13].

The prevailing methods for reducing feature sizes are predicated on the ability to cost effectively optimize one the three variables in the Rayleigh equation. This is achieved by optimizing one of the three main components to the photolithographic system:

(a) A reduction in the value of the resolution parameter, $\mathbf{k_1}$, results in higher resolution. However, contemporary manufacturing methods have already pushed this value to .4, and subsequent attempts at further reduction to the theoretical minimum of .25 have begun to yield diminishing returns. The resolution parameter is largely determined by current manufacturing capabilities and generally depends on a large number of tool, resist, and process parameters, the type of the mask and the pattern being imaged, as well as the requirements of the shape and allowed size range of the developed resist profile. Future attempts at further minimizing the resolution parameter begin to become cost prohibitive.

(b) Perhaps the main enabler in reducing feature size has been the implementation of shorter wavelengths of illumination, λ, (Figure 1.3). Unfortunately, one cannot indiscriminately select shorter wavelengths of radiation without meeting the necessary requirements that include both sufficient source power, and optical transparency of the transmission components. The push into the "extreme" ultra violet regime (<200 nm) has yielded a litany of technical obstacles including scarcity of high quality material and the transition to more expensive and complex reflective components.

Year	Linewidth (nm)	Wavelength (nm)
1986	1200	436 g-line mercury lamp
1988	800	436/365
1991	500	365 i-line mercury lamp
1994	350	365/248
1997	250	248 KrF excimer laser
1999	180	248
2001	130	248
2003	90	248/193
2005	65	193 ArF excimer laser
2007	45	193/157

Figure 1.3 History of radiation sources for photolithography.

(c) The final variable in the resolution equation that can be manipulated is an increase in the Numerical Aperture, **NA**, of the projection lens delivery system. For a given imaging system, NA = n sinθ, with n the index of refraction and θ being the half angle of incidence upon the wafer. With a fixed angle of convergence, researchers have successfully increased the NA by increasing the refractive index of the medium between the projection system (Figure 1.4) and substrate. The use of higher index fluids has spawned the field of Liquid-Immersion Lithography [14], which is poised to supplant existing exposure schemes in order to keep pace with industry milestones.

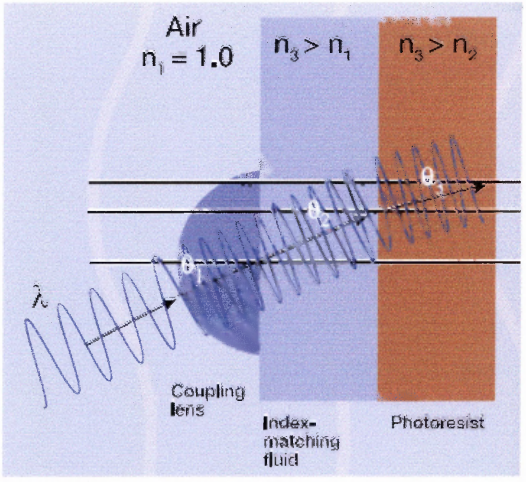

Figure 1.4 Schematic for immersion lithography [14].

The techniques for reducing feature size described above have resulted in the obtainment of the desired 45 nm node. However, future progression has encountered technical constraints including availability of optimum resist and source materials. This has lead to the investigation of complementary patterning techniques to extend the efficacy of conventional photolithography. One such technique, which utilizes existing processes, and is gaining significant interest is the field of Interference Lithography.

1.3 Wavefront & Amplitude Division Interference Lithography

The core of Interferometric Lithography (IL) is the instrument designed to exploit the interference of the light and the fringe pattern that ensues, the optical interferometer. An interferometer divides an initial beam into two or more parts, which travel different paths, and then recombine to produce an interference pattern. Interferometers are divided into two classes, delineated by the manner in which the initial beam is separated.

Amplitude-division interferometers (Figure 1.5) utilize a beam splitter, or pellicle, to divide the initial beam into two or more entities and then combine them later at a desired location. For lithographic applications [15], [16], amplitude-division interferometers

possess both attributes and detriments. Exposure times are substantially shorter, since most of the power is concentrated evenly into the two beams. This is an important factor when patterning in the nanometer regime, where shorter exposure aid in the suppression of air fluctuations and vibrations. Also, the amplitude-division interferometer enables the user to scan the wafer, allowing for large areas of exposure. The main detriment to the amplitude-division interferometer is the complexity and cost of the extra components, and the added feedback to ensure constant phase of the two beams. In addition, a change in period or resolution warrants a complete realignment of the system.

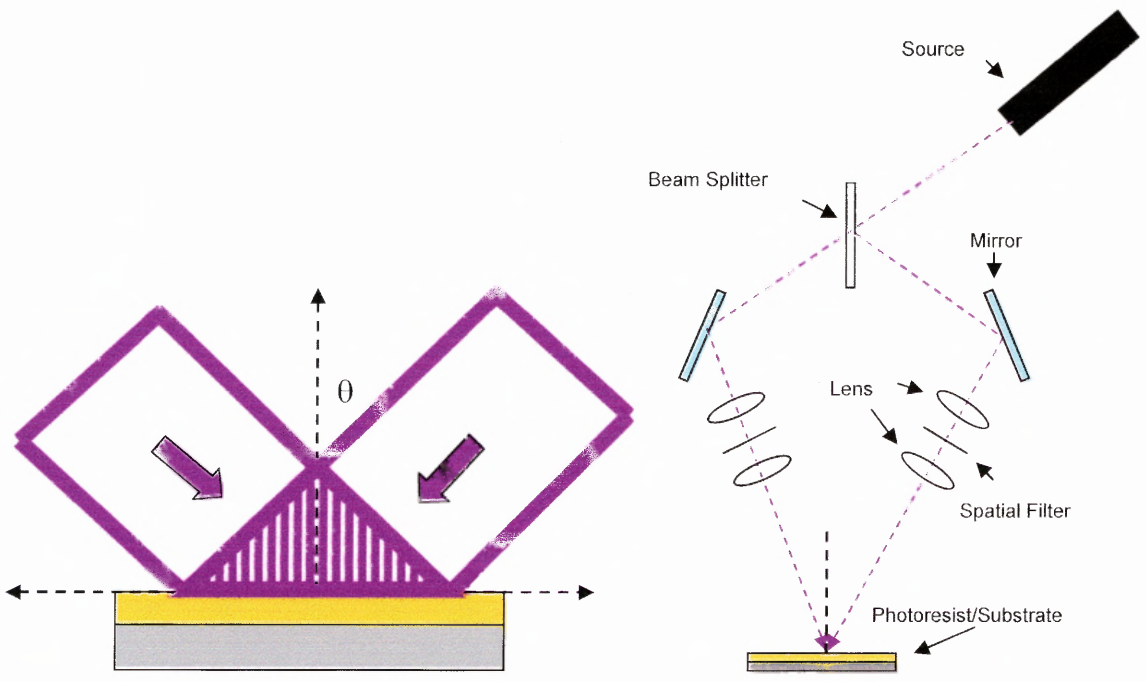

Figure 1.5 Amplitude-division interferometric lithography.

The second class of interferometer, and the one employed in this thesis, is a Wavefront division interferometer (Figure 1.6). These types of interferometers sample portions of the same wavefront of a coherent beam of light, commonly employing a

reflective or dispersive element. The fringe pattern is formed from the interference between the incident beam and a reflected portion of itself. Wavefront-division interferometers are a simple and mechanically stable method for nanopatterning [17]. Since the wafer/substrate is mechanically fixed to the mirror, the fringe pattern is not as sensitive to vibration. In contrast, an amplitude division interferometer typically employs sophisticated phase locking components two ensure that the two beams of the interferometer remain coherent during the exposure process. Having the two beams of the interferometer fixed to one another negates the need for any additional components. In addition, the wavefront division interferometer can be mounted on a rotation stage that allows for variable angle of incidence. By placing the axis of rotation at the intersection of the substrate and mirror, the period can be readily adjusted by changing the angle of incidence.

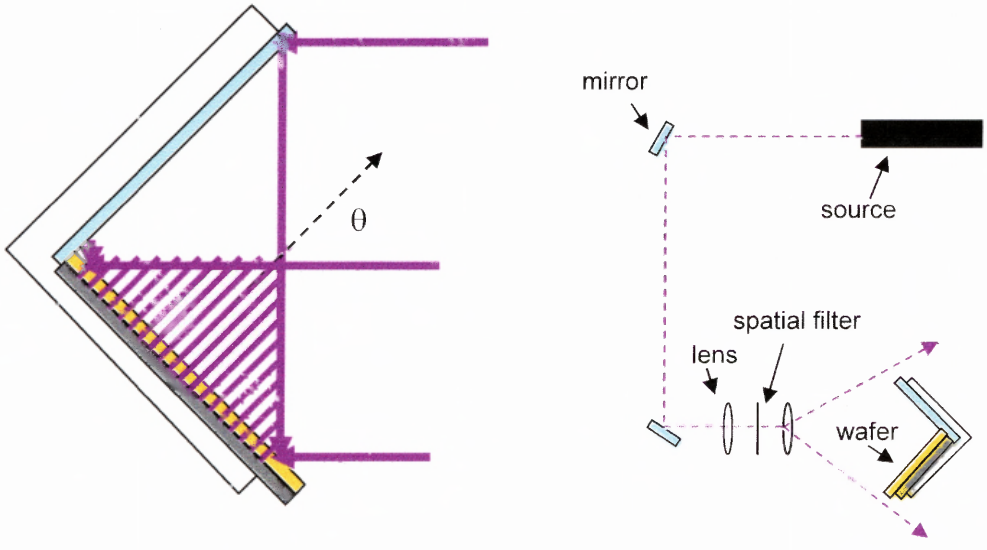

Figure 1.6 Wavefront-division interferometric lithography.

1.4 Organization of Thesis

In this thesis, the theory, fabrication protocol, and initial results of an alternative nano-patterning technique called Interferometric Lithography (IL) are presented. Comprised of the identical process attributes of traditional projection photolithography, IL mirrors the wafer preparation and development procedures of our existing clean room capabilities. The main departure is solely in means of pattern delineation. Interference Lithography is a "mask less" technique that employs the interference fringe pattern of two coherent beams, and can therefore, be generated with a commercial laser. Due to its simplicity, Interferometric Lithography provides an attractive supplement to existing methods of nano-patterning.

In the second chapter, the derivation of the interference equation and the resultant resolutions are provided. The contrast and coherence constraints are elucidated and a viable metric of visibility is determined for a specified exposure configurations. Later chapters encompass the fabrication of a Lloyd's Interferometer, initial experimental exposures, and quantification of dosage conditions. Finally, preliminary results are evaluated and conclusions are drawn to facilitate an effective protocol for future exposures.

CHAPTER 2

BACKGROUND

2.1 Two Beam Interference

The crucial element in the standard photolithographic process is the intricate photo-mask, which retains the desired pattern, and is imaged onto a prepared substrate. In Interferometric Lithography (IL) [18], the pattern or "mask" is the ensuing fringe pattern due to the interference of two coherent waves (Figure 2.1). Interferometric lithography (IL), allows considerable numbers of periodic structures to be patterned over a large area with short exposure times and standard lithography equipment. The resolution, or minimum feature size, becomes a function of the wavelength of exposure and the angle of impingement.

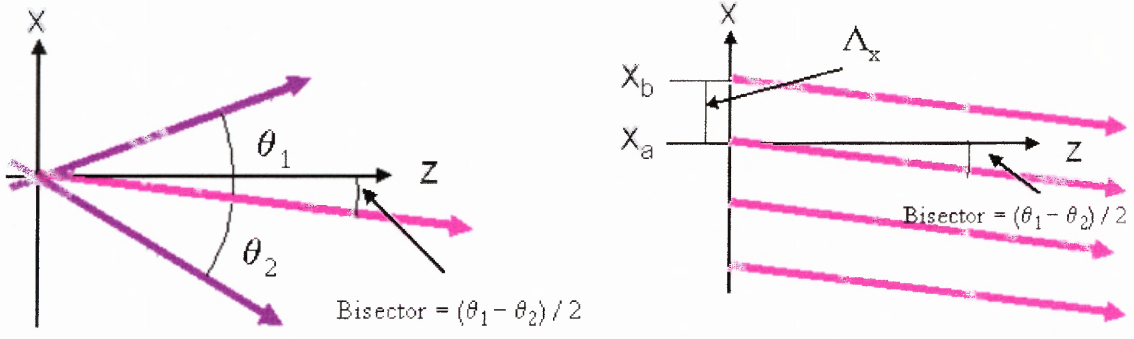

Figure 2.1 Two beam interference.

When two optical waves, Ψ_1 and Ψ_2, are present in simultaneous time and space, the intensity of this superposition is equivalent to the sum of each individual contribution and an interference term. The interference term is dependent on the phase difference

between the individual waves. Under specific conditions the phase argument dictates a subsequent intensity of periodic, spatially bright fringes due to constructive interference, and dark fringes due to destructive interference.

Analogous to traditional photolithography, the metric for successful patterning is intimately related to the transfer of the mask pattern. The efficacy of Interferometric Lithography is associated with the coherence of the interference pattern formed, and warrants a closer inspection to the factors that contribute to its integrity. Two waves are defined with respective phases, propagation and position vectors. The resultant irradiance is the modulus of the sum of the individual amplitudes. By substitution of the individual wave functions, their respective complex conjugates, and utilizing a trigonometric identity the total irradiance yields Equation 2.1, which is referred to as the Interference Equation.

$$\psi_1 = a_1 e^{i(k_1 \bullet r - \omega t + \delta_1)} \qquad k_1 = k(\sin\theta_1 \hat{x} + \cos\theta_1 \hat{z})$$

$$\psi_2 = a_2 e^{i(k_2 \bullet r - \omega t + \delta_2)} \qquad k_2 = k(-\sin\theta_2 \hat{x} + \cos\theta_2 \hat{z})$$

$$|\hat{x}| = |\hat{y}| = |\hat{z}| = 1$$

$$k = 2\pi / \lambda$$

$$I_{total} = |\psi_1 + \psi_2|^2$$

$$= |\psi_1|^2 + |\psi_2|^2 + \psi_1 \psi_2^* + \psi_1^* \psi_2$$

$$\boxed{I_{total} = I_1 + I_2 + 2\sqrt{I_1 I_2}\cos[(k_1 - k_2) \bullet r + (\delta_1 - \delta_2)]} \qquad (2.1)$$

It can be inferred from Equation 2.1, that the two factors which govern the total irradiance are the initial irradiance of each individual wave and the phase difference between them. The interference term will provide a positive or negative contribution, via constructive or destructive interference, depending on the sign of the phase argument, this occurs at integer values of π.

Determining the fringe spacing of the interference pattern provides the limit for the minimum attainable feature size. This is dependent upon the position vector and can be calculated by setting the resultant phase difference equal to a value of 2π. The fringe spacing, Equation 2.2, or minimum feature size, reduces to a function of λ, the wavelength of exposure and the sine of the angle, θ, between the two beams.

$$
\begin{aligned}
\Delta\phi &= \phi_b - \phi_a \\
&= [(k_1 - k_2)\bullet\hat{x}](x_b - x_a) = (k_1 - k_2)\bullet\hat{x}\Lambda_x \\
&= [k\sin\theta_1 - (-k\sin\theta_2)]\Lambda_x \\
&= k[\sin\theta_1 + \sin\theta_2]\Lambda_x \\
\Delta\phi &= 2\pi \\
2\pi &= 2\pi/\lambda[\sin\theta_1 + \sin\theta_2] \\
\lambda &= [\sin\theta_1 + \sin\theta_2]\Lambda_x \\
\Lambda_x &= \lambda/\sin\theta_1 + \sin\theta_2
\end{aligned}
$$

$$
\boxed{\Lambda_x = \lambda/2\sin\theta} \qquad (2.2)
$$

The capacity to attain sub micron features, with even visible wavelengths, makes Interference Lithography a very attractive technique for nano patterning. Figure 2.2

illustrates the achievable periods for corresponding angles of exposure and for a variety of contemporary sources. For normal incidence the period converges to a value of half the wavelength of exposure. However, this is deceptive since the area of exposure reduces to an ineffectual amount. The geometry of the optical configuration dictates both the integrity of the fringe pattern and the area of exposure, and therefore the period resolution. For higher density structures, a limit of 60 degrees is more realistic for adequate exposure conditions.

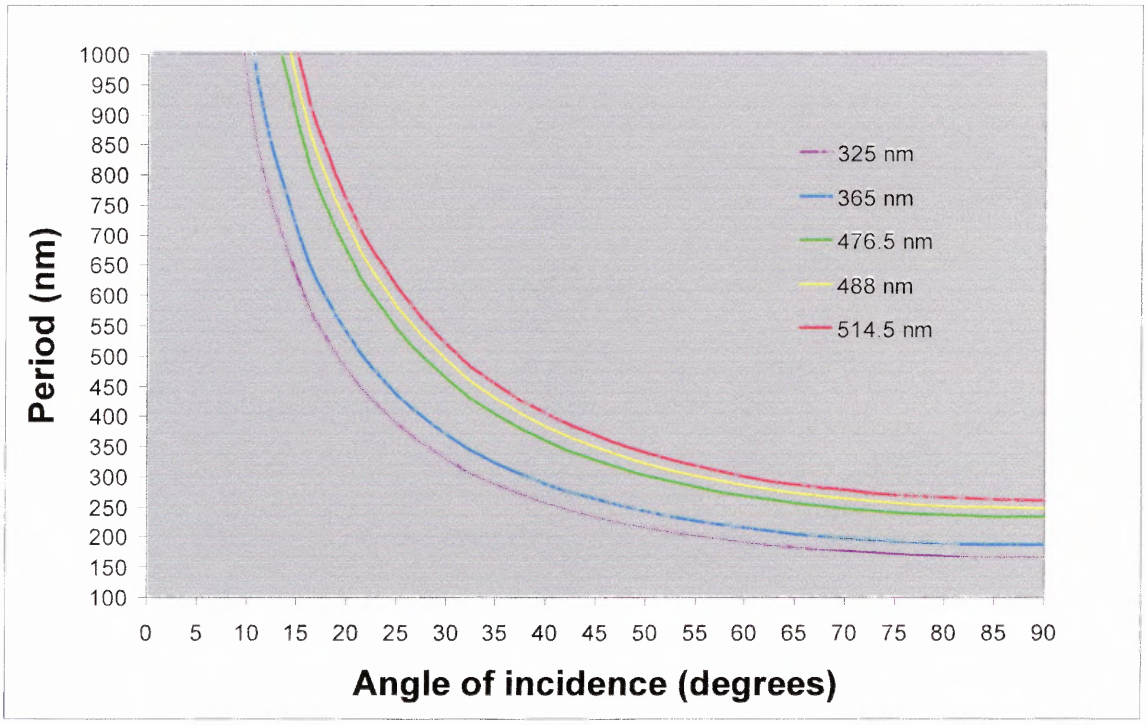

Figure 2.2 Minimum feature sizes for a range of chromatic sources.

2.2 Fringe Visibility

If it is assumed that the interference that arises is from two completely coherent beams, then any contribution originating from phase correlation function, γ_{12}, can be negated. The interference term yields either constructive or destructive interference, Equation 2.3, when the phase argument becomes 1 or -1. The resultant intensity of the interference (Figure 2.3), takes on a cosine pattern with peaks corresponding to intensity maxima, and valleys for intensity minima. When the individual intensities are equal to each other, the interference pattern yields a maximum value of 4I and a minimum at 0. A variation in individual intensities, relative to one another will result in a decrease in the intensity maximum and an increase in the minimum. These variations can play a significant role in the overall exposure dose and later influence the fidelity of the grating pattern.

$$I_p = I_1 + I_2 + 2\sqrt{I_1 I_2}\,\mathrm{Re}\left[\gamma_{12}(\tau)\right]$$
$$I_{\max} = I_1 + I_2 + 2\sqrt{I_1 I_2} \qquad (2.3)$$
$$I_{\min} = I_1 + I_2 - 2\sqrt{I_1 I_2}$$

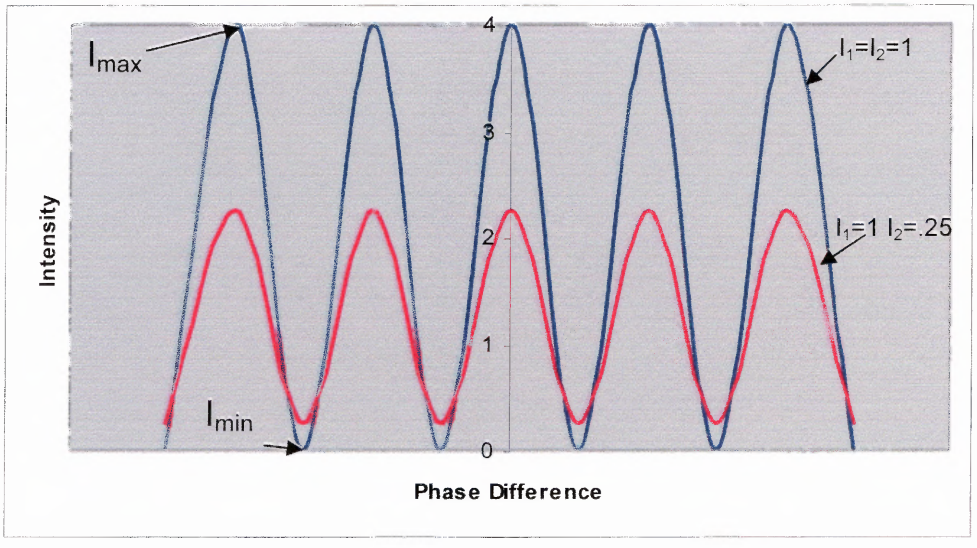

Figure 2.3 Plot of resultant intensity due to interference.

The metric used to represent the measure of interference strength, that occurs between two beams is the, fringe visibility. The visibility or contrast, Equation 2.4, encapsulates any variation between the intensities of the two beams and the resultant intensity that arises from their interference. In addition, the phase variations or coherence will contribute to the overall contrast as well.

$$Visibility = \frac{I_{max} - I_{min}}{I_{max} + I_{min}} \mathrm{Re}\left[\gamma_{12}(\tau)\right] \tag{2.4}$$

$$Visibility = \frac{2\sqrt{I_1 I_2}}{I_1 + I_2} \mathrm{Re}\left[\gamma_{12}(\tau)\right]$$

The visibility or fringe contrast determines the efficacy of the pattern transfer during the exposure process. Since the interference fringes serve as a mask to delineate the grating structure, it is imperative that the fringes have the highest contrast possible. The ideal case results from equal individual intensities and complete coherence. A high contrast exposure results in the photoresist receiving a uniform dose of the fringe pattern irradiance. This is a prerequisite to achieve a structure of high integrity. For completely coherent beams, the visibility reduces to a function of the individual intensities, and decreases as these values begin to differ.

It can be seen that the visibility remains high as a function of relative intensities, even when there is a rather large disparity in the individual values (Figure 2.5). Therefore discrepancies in the relative power do not have as large an effect on the contrast of the pattern. Even a relative intensity of .5 still yields a visibility of almost 90%, assuming the system is void of any other influences that may affect the individual beams. Despite additional restrictions, this forgiving attribute allows relatively high fringe contrasts for

considerable ranges in individual intensities and is a motivating factor in employing interferometric lithography for nanopatterning.

Despite the fact that the contrast may remain high over these variations, the photoresist response to illumination will ultimately dictate the integrity of the overall grating structure. A variation in contrast manifests itself as a non uniform dose that the resist receives. Any non uniformity in exposure constitutes an eventual inhomogeneity in the resultant chemical structure of the resist. This inhomogeneity can be exacerbated during the post exposure processes, such as development and bake treatments. Therefore, it is not wholly conclusive that a high interference fringe contrast alone will result in an optimal pattern.

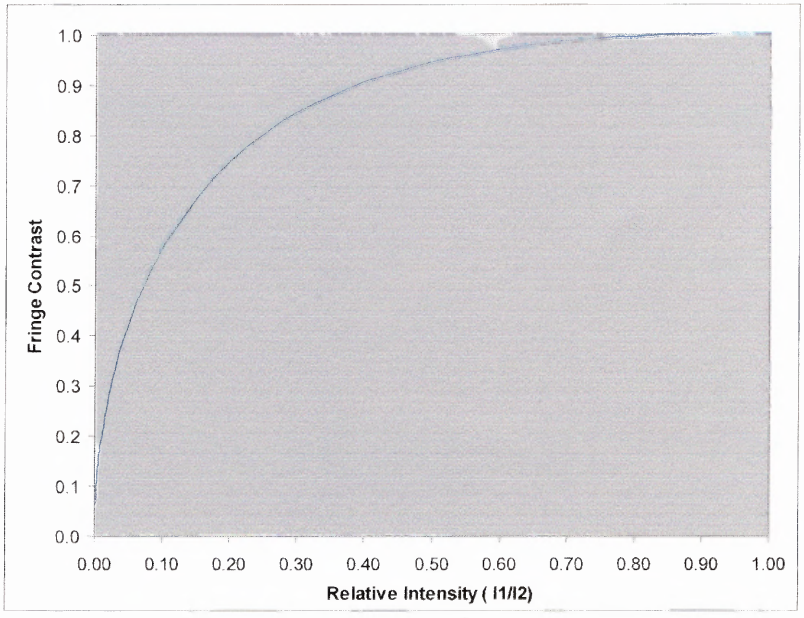

Figure 2.4 Visibility as a function of relative beam intensity.

It was shown earlier that a discrepancy in individual beam intensities will manifest itself as a decrease in fringe contrast or visibility. However, such a result was predicated

on the argument that the two beams where completely coherent. The interference equation dictates that in addition to intensity effects, the phase variations that ensue will limit the visibility and therefore the area that can be patterned. The influence of coherence effects warrants a closer examination.

Optical radiation propagating from a laser source will never be completely monochromatic. Rather, the emitted light can be represented as a sequence of harmonic wavetrains of varying finite length, Figure 2.6, each separated from each other by a discontinuous change in phase. These fluctuations arise from the atomic nature of the gain medium and the erratic transitions that can occur between intrinsic energy levels. A given source is therefore characterized by an average wavetrain lifetime, commonly referred to as the coherence time, τ_0. From the coherence time the corresponding coherence length, l_t, of a coherent pulse can be determined.

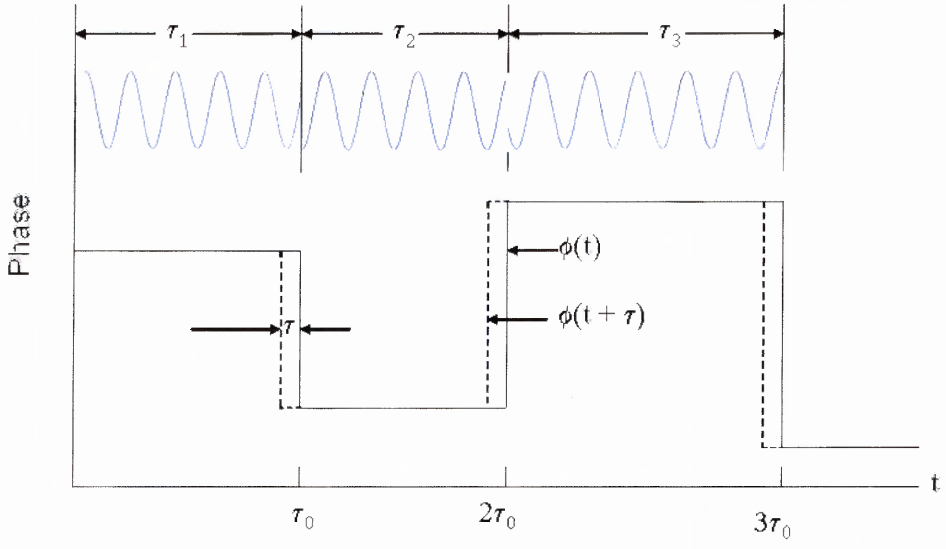

Figure 2.5 Sequence of harmonic wavetrains of varying finite lengths or lifetimes τ.

It is well understood that interference results from the spatial overlap of two beams emitted from the same source. The difference in distances that each path takes before recombining sets a limit for the geometry of the interferometer. This path distance difference must be less than the coherence length of the laser. Therefore, the length over which the beam is classified as coherent dictates the length of each individual arm of the interferometer. Since it is necessary to maintain high fringe contrast, a relationship between visibility and coherence length can be elucidated.

In amplitude division interferometers, the arms are mechanically independent of each other and path differences can be monitored and adjusted without affecting the complementary beam. This necessitates the need for the ability to monitor the contrast fringes of the system and adjust the overall visibility. Researchers have utilized this technique for delivering variable exposures in order to characterize resist kinetics and process latitudes [19]. Despite this geometric independence, the lack of mechanical stability of each arms in relation to one another warrants a means for locking the individual phases. This is not the case when using wavefront division interferometers for interference lithography. Since each arm is mechanically fixed in the interferometer, the system serves to stabilize any vibration or environmental induced distortion to the beam. However, the gain in mechanical stability comes with a cost in the path length of each arm. The optical path difference is only zero at the point of intersection between mirror and substrate. The points of exposure at distances greater than at the point of intersection, the path difference between the beams increases and the contrast degrades (Figure 2.7). The geometry of the interferometer, in relation to the coherence length of the source, sets the overall area of exposure.

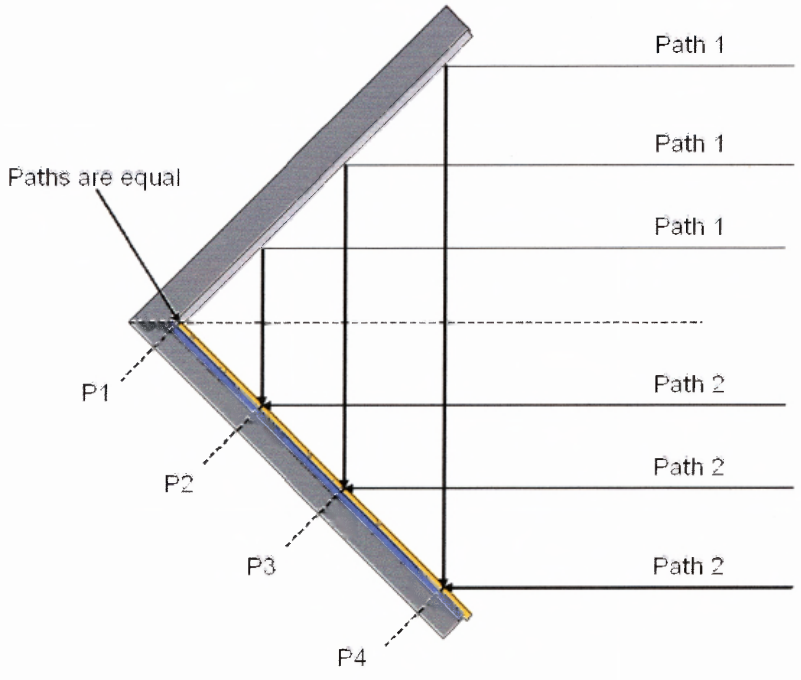

Figure 2.6 Representation of optical path difference for wavefront division interferometer.

The relative variation in individual beam intensities is not the only factor that determines the overall visibility. The interference term can add to or subtract from the simple sum of the two beam irradiances depending on the correlation in phase between the two beams at the point of interference. A correlation function, Equation 2.5, is defined to represent the phase variation between the two beams, dividing by the amplitudes of the two beams results in the normalized correlation function, Equation 2.6.

$$\Gamma_{12}(\tau) \equiv \left\langle E_1(t) E_2^*(t+\tau) \right\rangle \tag{2.5}$$

$$\gamma_{12}(\tau) \equiv \frac{\Gamma_{12}(\tau)}{\sqrt{I_1 I_2}} \tag{2.6}$$

The fringe contrast is also dictated by the degree of coherence between the two beams. When the individual intensities are equal in magnitude then the resultant interference intensity becomes solely a function of the normalized correlation function. The dominant term of the interference term is a function of the time interval, τ, and therefore the location of interference. It is known that the time difference between paths, relative to the average coherence time of the source, is crucial to the degree of coherence achieved. At some difference in interference point, the accompanying time interval will be greater than the coherence time dictated by the source. This will result in some coherence being lost. Therefore, the normalized correlation function reduces to a function of the time interval and the intrinsic coherence time (Equation 2.7). The resultant fringe contrast will therefore be a function of the degree of coherence between the two individual beams. The variation in degree of coherence can be directly related to the difference in the location of the point of interference. Since it is known that the coherence time and coherence length scale by factor of the speed of light, c, and then the correlation function can be written as a function of optical path difference and intrinsic coherence length of the source (Equation 2.8).

$$\left|\gamma_{12}(\tau)\right| = 1 - \frac{\tau}{\tau_0} \tag{2.7}$$

$$\left|\gamma_{12}(\tau)\right| = 1 - \frac{\Delta}{l_t} \tag{2.8}$$

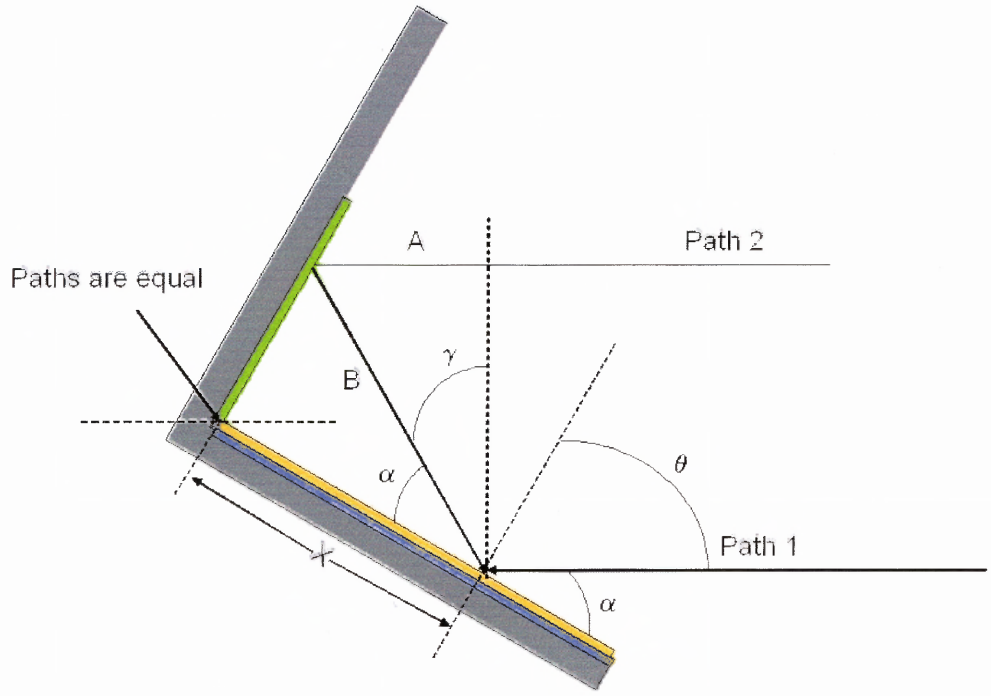

Figure 2.7 Geometric determination of optical path difference.

$$\begin{aligned} \text{Optical Path Difference} &= \text{Path 1} + \text{Path 2} \\ &= \text{Path 1} + (A+B) \\ &= (x / \cos\alpha)\,[1+\sin\gamma] \end{aligned} \tag{2.9}$$

It was assumed from the interference equation that the visibility reduces to a function of the individual irradiances when the phase difference between the two beams is equal to 1. A constant phase difference implies that the path length that each beam travels to the point of interference is held constant. The magnitude of optical path difference between the two lengths sets the limit on the fringe visibility. Coherence is lost when the optical path difference between the lengths that each individual beam travels to get the point of interference is greater than the coherence length of the laser. Therefore, the

coherence length of the laser source dictates how large an area the visibility remains high and consequently how large an area that can be exposed effectively. The geometry of the wavefront division interferometer determines the optical path lengths that each beam will travel before interference. The geometry becomes a function of the angle of incidence, which in turn is a function of period of the grating exposure. An optical path difference, Equation 2.9, arises when the angle of incidence is varied due to the two portions of the wavefront impinging at different points on the interferometer.

With the coherence length of the source equal to 30 cm, the visibility for a given period exposure will decrease at points increasing in distance from the intersection of mirror and substrate (Figure 2.7). Therefore, as the period increases in resolution, a function of incident angle, the area of exposure decreases. In order to achieve smaller feature sizes, approaching the lower limit of interference lithography, the useful area of exposure and density must be sacrificed.

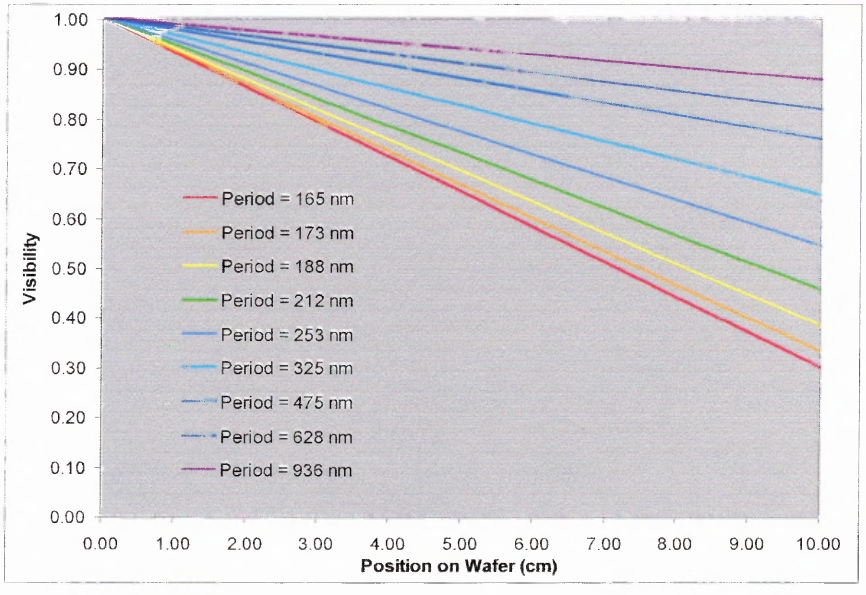

Figure 2.8 Visibility as a function of optical path difference.

2.3 Line Edge Roughness

The smallest feature discernable in a given patterning process is referred to as the resolution. The resolution of a patterning process can be defined as the photoresist's response to a given modulation or MTF. In lithographic applications the patterning process is composed of two components; exposure and development. The efficacy of the patterning process is dictated by the resolution of the exposure pattern, termed the visibility, and the resolution of the photoresist itself. As discussed earlier, the resolution or visibility of the exposure pattern is dictated by the factors that contribute to the interference equation. The resolution of the photoresist is closely related to both the physicochemical response to the optical radiation during exposure, and the subsequent effects during the development process. Post exposure influences, that degrade the overall structural integrity of the desired resist pattern, are a result of the chemical composition of constituent components of the development process. Factors include developer concentration, temperature, agitation, and degree of saturation. The resultant effects due to variation of these components manifest themselves greatly when patterning smaller and smaller features. A tolerance can be established that dictates an acceptable structural defect that may arise during the patterning process. The magnitude of these defects establishes a pass/fail criterion for a given result.

The effectiveness of using the periodic fringe pattern of an optical interferometer for pattern delineation is intimately related to the contrast between the fringes, or visibility. Variations in the incident pattern intensity, resulting from a loss in visibility, lead to an inhomogeneous exposure. This gives rise to a stochastic response by the photoresist, with multiple chemical variables determining the overall performance and mechanical integrity

of the grating. Variations in the chemical response of the resist manifest themselves as structural imperfections, Figure 2.7, when developed and assume a significant portion of the desired feature [20]. A quantifiable metric, representing these structural imperfections, and thus assessing an acceptable result has been termed line-edge roughness (LER).

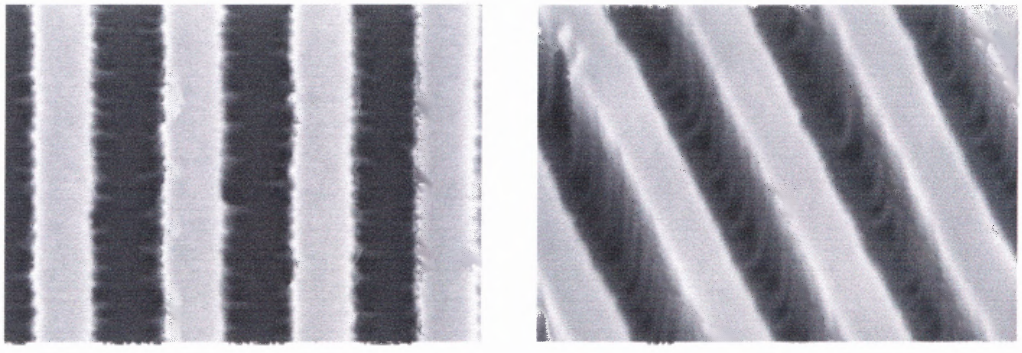

Figure 2.9 SEM image of Line Edge Roughness of periodic pattern [20].

Line edge roughness (LER) is a term that encapsulates the random fluctuations in the width of a resist feature that are due to variations of the molecular structure and weight of the resist polymer. The variations of theses intrinsic components lead to non linear values of the photoresist's resultant solubility during further development processes. The factors that influence the resist's final solubility are directly related to the magnitude of the incident optical exposure. The maximum of the image exposure render regions of the resist that are highly soluble, while the corresponding minimums result in regions that are insoluble. During an intermediate exposure dose, the solubility alters between these two extremes. A spatial inhomogeneity of resist solubility will arise from an inhomogeneous exposure to optical radiation. When the resist is developed, a corresponding structural inhomogeneity will result and is encompassed as LER.

Technologies incorporating next generation nano-patterned media necessitate a quantitative assessment of the chemically amplified photoresist used to lithographically define sub-micron dimensions. The magnitude of LER can be correlated to the contrast or visibility of the exposure pattern [21], [22]. As the fidelity of the pattern decreases, via variable contrast, irregularities ensue due to stochastic processes resulting in a roughening of the structure edges. These irregularities are a direct consequence of a non uniform exposure to the desired radiation.

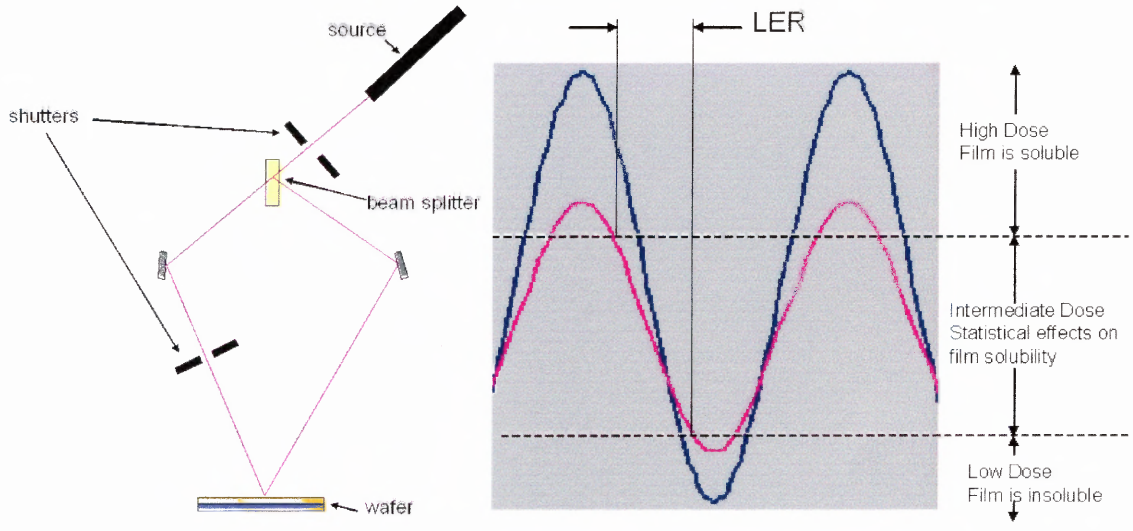

Figure 2.10 Interference lithography for intermediate exposure dose delivery [23].

Interference lithography (Figure 2.8) serves as a powerful tool for delivering variable exposures of intermediate doses to the photoresist [23]. Variable contrast can be achieved by controlling the factors that decrease visibility, such as inequality in individual irradiances and optical path length difference of the exposure geometry. The employment of an amplitude division interferometer was utilized for delivering exposures of variable contrast. The magnitude of the fringe pattern can be adjusted by obstructing or prolonging

the exposure radiation from both the arms of the interferometer. Interference lithography provides a means to vary the magnitude of the incident interference pattern in a controlled manner. A tandem exposure protocol, Figure 2.9, was utilized for effectively controlling the magnitude of the exposure dose. A full fringe exposure of varying intensity was delivered first, followed by exposing the sample to a broad flood exposure. This serves to effectively vary the amplitude of the peaks and troughs of the resultant intensity pattern and deliver an exposure in the intermediate regime. An intermediate dose results in the resist's solubility being dominated by statistical effects. These statistical effects manifest themselves as chemical inhomogeneities and give rise to corresponding structural irregularities or LER.

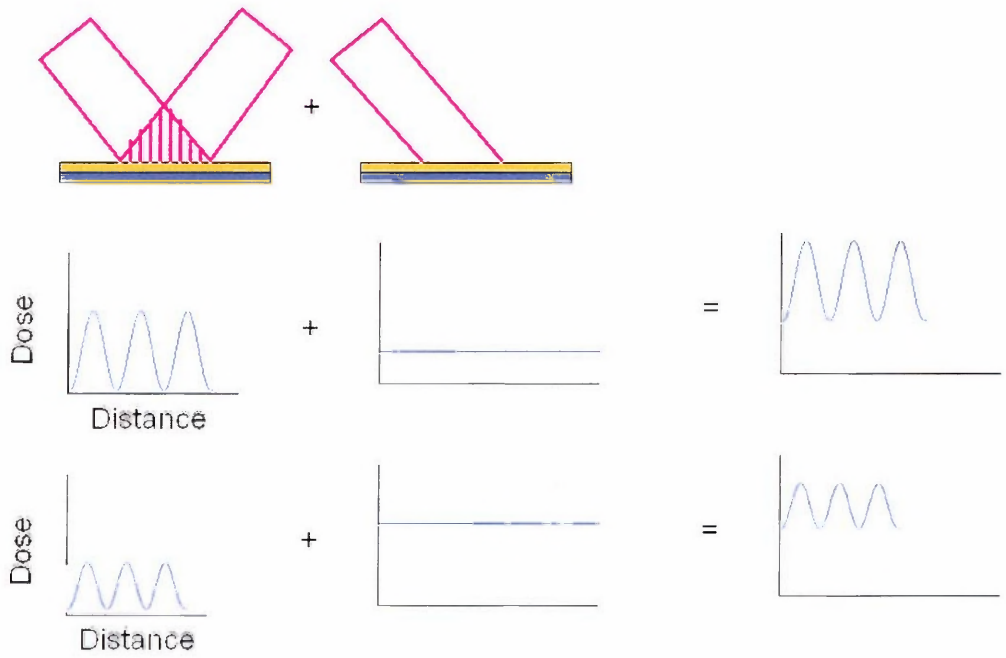

Figure 2.11 Tandem exposure protocol for controlled contrast of variable intensity [23].

The amplitude of these irregularities or line edge roughness can be correlated to specific degrees of varying contrast. Adjustable dosage, achieved through a tandem exposure protocol, result in variable exposures in the intermediate regime. The statistical effects on the resist solubility are depicted in the corresponding SEM images, Figure 2.10. It is interesting to note that though the amplitude of LER can be a significant fraction of the resist feature, the line width of the structure remains constant. Therefore, size or pitch of the resultant pattern will maintain periodic despite the loss of exposure contrast. Variations in the fringe visibility will manifest themselves strictly as LER.

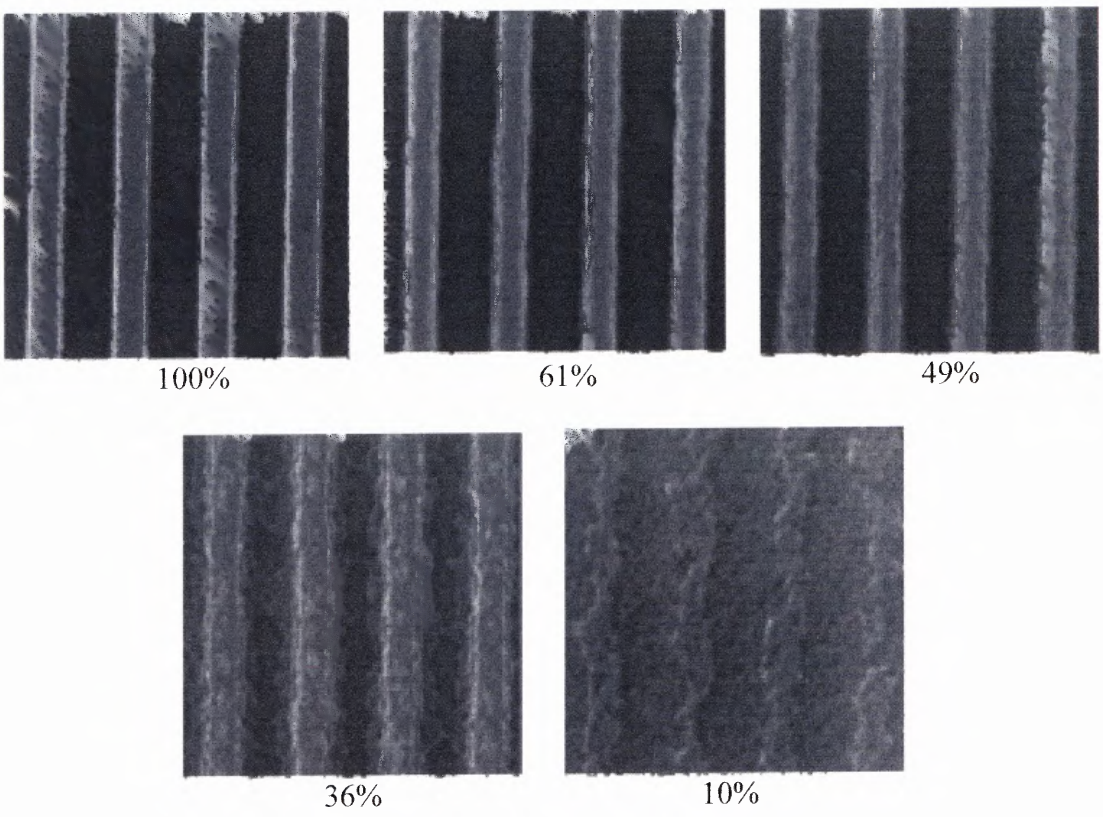

Figure 2.12 Line Edge Roughness, (LER) of positive photoresist for exposures of varying degrees of contrast [23].

CHAPTER 3

IMPLEMENTATION OF INTERFERENCE LITHOGRAPHY

3.1 Experimental Setup

The initial effort at implementing interference lithography sought to utilize an amplitude division interferometer. The intrinsic attributes of the system include the ability to scan the wafer across an extremely flat surface, i.e. the optics table, and conserve optical power by keeping the beams close to collimated. By keeping the geometric loss to a minimum, the exposure times can be kept relatively short, therefore reducing any environmental effect on the beam quality. It is imperative that disturbances are minimized so that any aberrations in the incident beam will not manifest themselves in the final relief structure. Despite initial implementation attempts, the system required additional components which increased both the complexity, and geometric foot print. In addition, methods to improve stability proved cost prohibitive and the amplitude division interferometer was abandoned.

A hybrid optical configuration (Figure 3.1) was constructed that aimed to incorporate the attributes of the amplitude division interferometer, while negating the need for any additional components. A scanning wavefront division interferometer was developed that sampled the same portion of the wavefront, as in traditional configurations, but illuminated the sample from a vertical position. This enabled the arms of the interferometer to be fixed while allowing for the wafer to be displaced. The optical configuration utilized a 325 nm, HeCd source from Kimmon Electric Ltd. This single mode laser offers a robust package with a coherence length of 30 cm and an output power of 25 milliwatts. A pair of dielectric mirrors was used to steer the beam to a keplerian beam

expander that was aligned off axis. The beam expander is composed of lens for focusing the beam, a spatial filter to remove imperfections induced from the optics, and an additional lens to diverge the beam.

Although initial efforts appeared positive, upon closer inspection the final exposures showed that the grating structures were degraded. The inconsistencies were likely the result from a non uniformity in the beam intensity. The geometry of the system, due to off axis illumination, constrained the beam divergence and the width of the gaussian distribution was smaller than the sample exposure. This resulted in the substrate receiving a non uniform dose and subsequently a sub-optimal exposure. In order to mitigate the ill effects from the non uniformity, the scanning setup was abandoned for a traditional Lloyd's interferometer (Figure 3.2). This provided additional distance for the beam to diverge and ensure that a uniform intensity was incident on the sample.

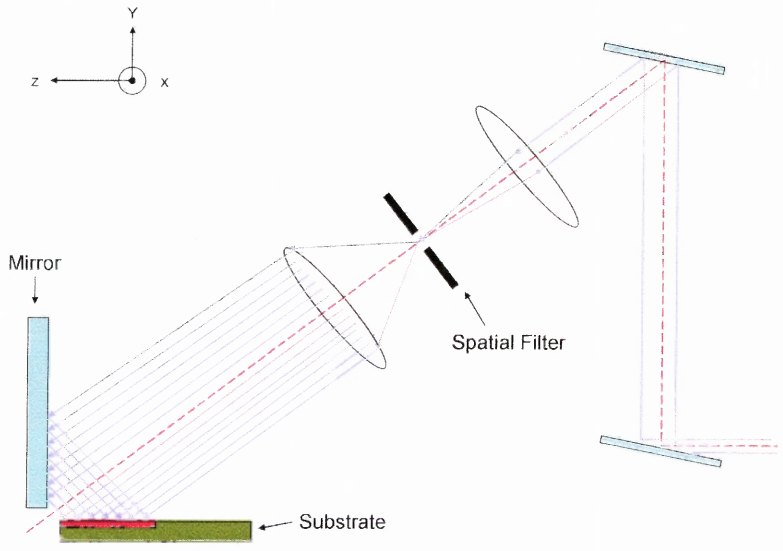

Figure 3.1 Initial configuration for scanning wavefront division interferometer.

Given the constraints described previously, the Lloyd's wavefront division interferometer was a logical progression for optical configurations. The wafer/substrate can be mechanically fixed to a 25.4 mm dielectric mirror, ensuring greater stability, but consequentially fixing the area of exposure. The final patterned area is constrained by the optics used to form the interference pattern. This is in contrast to amplitude division interferometers which enable the wafer to be scanned, providing a much larger area of exposure. A rotation stage, with axis of rotation at the intersection of the mirror and substrate, was implemented to allow for variable angles of incidence. Exposure of different periods can be attained by rotating the mirror/substrate about its axis.

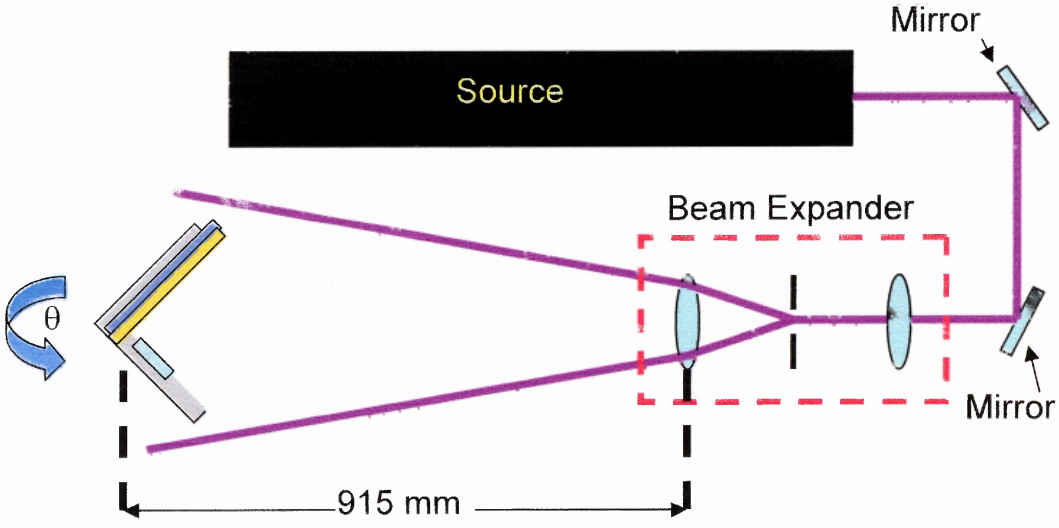

Figure 3.2 Optical configuration for wavefront division interferometric lithography.

The wavefront division system is not without its own shortcomings. Though, the integrity of the beam does not suffer environmental induced gradients and phase drifts. The wavefront is eventually aberrated, since the last components before interference are a lens for expansion and the dielectric mirror. It is illogical to have any optical elements after the

spatial filter that could reintroduce noise and aberrations into the beam. However, since the overall optical foot print was limited, an additional lens was required to expand the beam and a reflective element will always be the final optic in a wavefront division system. The beam expander ensured that the area of exposure was uniform over the desired area which is dictated by both the size of the elements, and the final period desired.

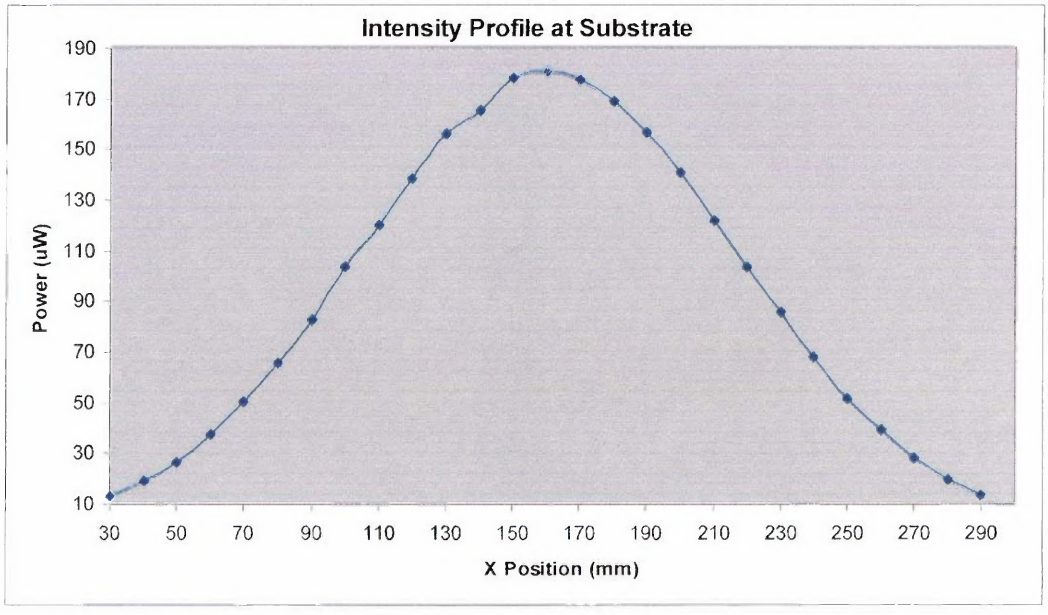

Figure 3.3 Intensity profile at location of substrate.

To ensure a uniform exposure, it is imperative that the illumination beam propagate an adequate distance. This serves multiple purposes allowing the beam to be approximated as a plane wave. A plane wave approximation is a prerequisite for the interference equation and subsequent fringe spacing. A long divergence also ensures that the wafer/resist receive an equal amount of radiation and thus a uniform exposure. The beam propagation is limited only by the geometric constraints of the configuration, i.e., table length. However, it is also important to maximize the intensity at the substrate plane in order to keep exposure times

as short as possible. A proper balance must be met in order to ensure both uniform and short exposures, the longer the exposure the more susceptible to vibration and thermal gradients. For the exposures performed in this research, the beam (Figure 3.3) was allowed to diverge so that the 13.5% points of the gaussian profile fell well past the area of interest equivalent to roughly twice the size of the mirror or 50 mm.

In addition, to the increased exposure times, the wavefront division system is subject to geometric constraints. Depending on the angle of incidence, the area of exposure will vary in size (Figure 3.4). For smaller angles of incidence the effective area of exposure decreases. In an effort to decrease the exposure time, the divergence of the beam was tightened leading to a smaller area of uniform intensity. This meant that the area of exposure had to be sacrificed since a homogeneous beam is a requirement for a uniform dose. By minimizing the exposure area; the visibility remained high over the whole exposure. This ensured that the substrate received high contrast and would not be subject to any deleterious effects due to inconsistencies in the fringe pattern.

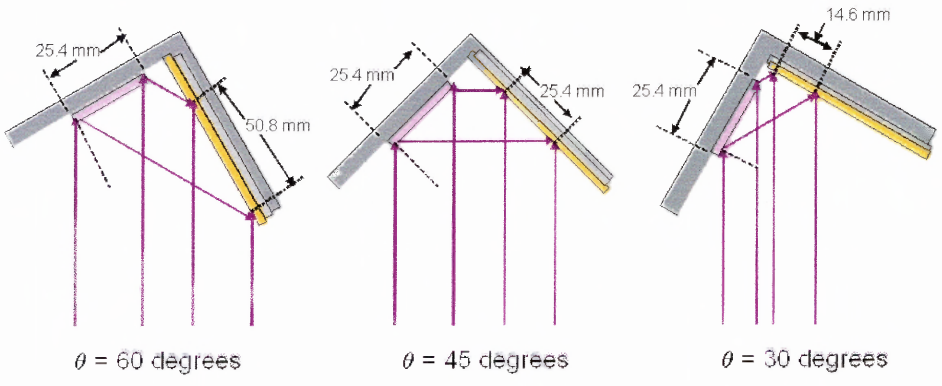

Figure 3.4 Geometric constraints of exposure area with varying angle of incidence.

3.2 Dose Quantification

The substrate samples were prepared using standard photolithography cleaning (DI water & isopropyl) and photoresist deposition methods. After the P-clean bath the wafers were placed on the spin coater and Shipley 1805 positive photoresist was deposited at a revolution speed of 5000 rpm for 60 seconds. Following a post bake for 60 seconds at 115°C, a uniform coating of 500 nm was verified using a Rudolph ellipsometer.

Determining the optimum exposure time was a complex issue that was confounded by the fact that Shipley 1805 series resist, is designed to be most responsive to radiation in the range between 350 nm to 450 nm. The manufacturer's data, Figure 3.5, calls out a sizing energy of 150 mJ/cm^2 (milliwatts*seconds/cm^2), for a given resist thickness of 1.23 um, and exposure at a wavelength 365 nm. The exposure time (seconds) is derived by dividing the sizing energy by the available power (watts) at the substrate.

MICROPOSIT S1813 PHOTO RESIST
with MICROPOSIT MF-321 DEVELOPER
Table 2. Functional Lithographic Summary Data

Process Parameters (Refer to Figures 5 and 6)	
Substrate	Quartz
Coat	12,300Å
Softbake	115°C/60 seconds Hotplate
Expose	Oriel Scanning Wedge
Measure	Hewlett Packard 8450A Spectrophotometer

Sizing Energy	150 mJ/cm^2 (1.3 E_0)	
Resolution	0.48 µm	
Masking Linearity (±10% CD)	0.50 µm	
	1.0µm L/S	0.60 µm L/S
Exposure Latitude (±10% CD)	65%	45%
Focus Latitude (±10% CD) ≥ 85° Wall Angle	2.25 µm	1.25 µm

Figure 3.5 Shipley 1800 series positive photoresist process and exposure parameters.

The system in this research utilized 325 nm exposure and a resist thickness of 500 nm. Initial exposures attempted to determine exposure times by simply extrapolating the

resist response at 325 nm using Shipley data. In addition, a linear relationship was assumed for the exposure time versus resist thickness. Both assumptions proved to be inaccurate as the response of the resist is highly nonlinear, and an alternative method utilizing empirical results, was used to determine viable exposure times.

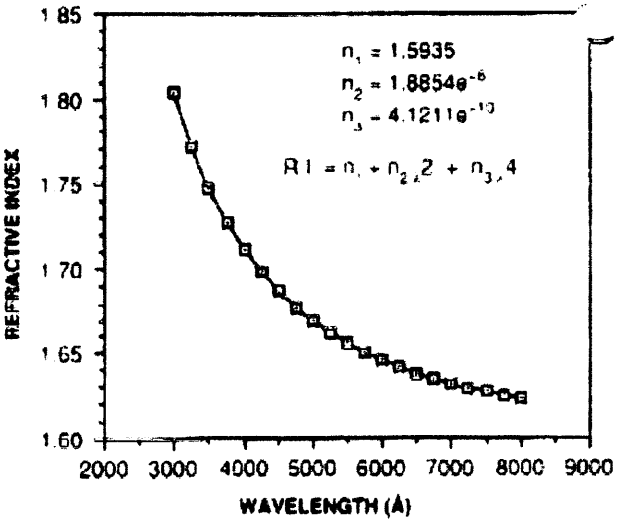

Figure 3.6 Dispersion curve for Shipley 1800 series positive photoresist.

In order to accurately determine the optimum exposure time, the actual intensity that the photoresist receives must be determined. Whenever optical radiation encounters an interface of a different index of refraction a Fresnel reflection, or loss, ensues that detracts from the incident intensity. Using the correct index of refraction of the Shipley 1805 resist, Figure 3.6, the amount of light transmitted into the film can be calculated for a given incident angle. Snell's law was utilized in order to determine the angle of the transmitted radiation into the resist. The transmitted angle can then be incorporated into the Fresnel equation, and the amount of radiation that couples into the resist can be determined as a

function of angle. The Fresnel loss values, Figure 3.7, represent one of the factors that must be taken into account when quantifying the exposure time.

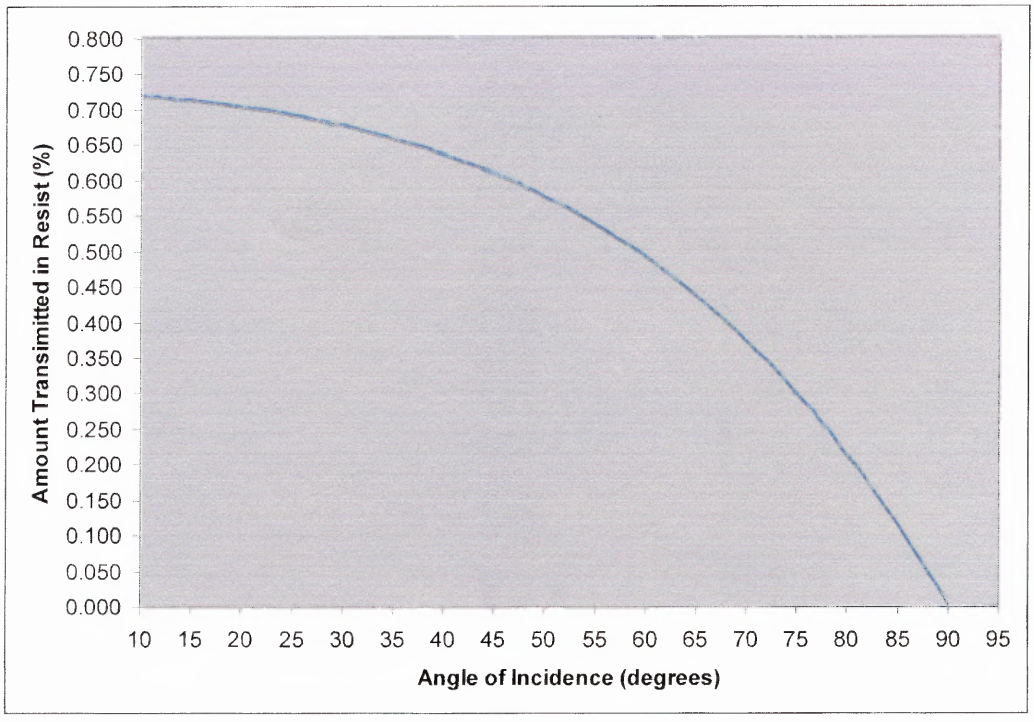

Figure 3.7 Percent of incident radiation transmitted into resist due to Fresnel loss.

In addition to the Fresnel loss associated with the change in index, the response of the resist to 325 nm radiation must be determined. The manufacturer data specifies exposure conditions on a fixed resist thickness of 1.23 um and incident radiation of 365 nm. Rather than extrapolate the data and estimate the corresponding exposure time, the absorbance spectrum of the Shipley 1805 resist, Figure 3.8, can be used to determine the intensity of the radiation absorbed. By utilizing the Beer-Lambert Law to empirically relate the absorption of light to the properties of the material it is traversing through, a value for the intensity absorbed can be determined and used to derive an exposure time. This absorbed intensity, in conjunction with the actual incident radiation, including Fresnel

loss, will provide the value for the optical power that is available for exposure. The actual power can then be used to calculate the exposure time which will become a starting point for initial radiation dosage.

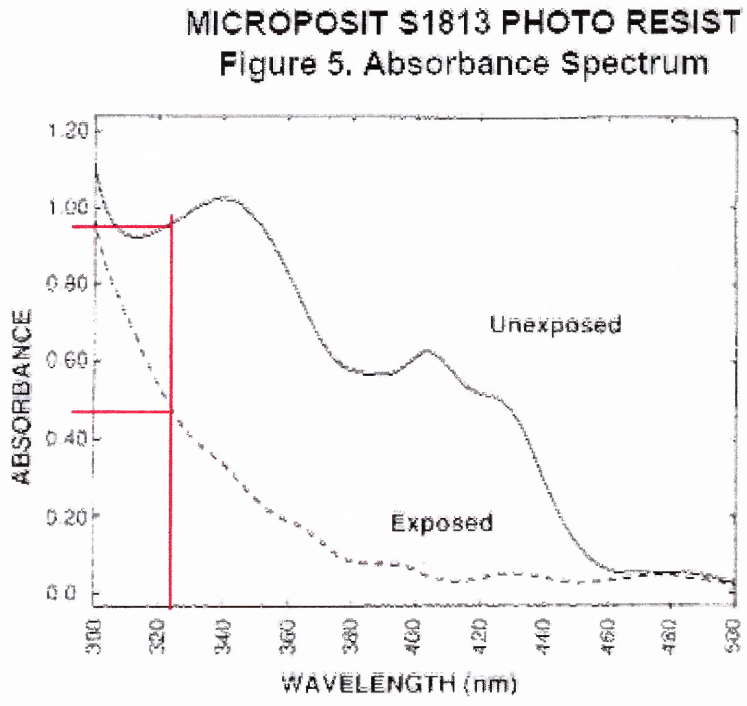

Figure 3.8 Absorbance spectrum of Shipley 1800 series photoresist.

The Shipley absorbance data can be used to determine the amount of radiation absorbed by the resist for a given thickness. The absorbance spectrum indicates that the Shipley 1805 does have somewhat of a response at 325 nm. As the curve depicts the resist has an absorbance, i.e., the difference between unexposed and exposed points, of roughly .5 or 50%, for a thickness of 1.23 um. It was assumed that all values are for a fixed film thickness specified by the manufacturer. This value in conjunction with a fixed thickness can be inserted into the Beer-Lambert formula, Equation 3.1, and the absorption coefficient can be determined. The absorption coefficient is then used to determine the absorbed

intensity, I_{abs}, for any variation in resist thickness and any given initial intensity, Io. The initial intensity is determined by the available power at the substrate including the Fresnel loss. The exposure time, Equation 3.2, is then the sizing energy, provided by the manufacturer, divided by the absorbed intensity and a value in seconds is determined.

$$\begin{aligned} I(x) &= I_0 e^{-\alpha x} \\ I_{Abs} &= I_0 - I_0 e^{-\alpha x} \\ &= I_0 (1 - e^{-\alpha x}) \end{aligned} \tag{3.1}$$

$$\text{Exposure Time (secs)} = \frac{\text{Sizing Energy (milli Joules/cm}^2\text{)}}{I_{abs}\text{(micro Watts/cm}^2\text{)}} \tag{3.2}$$

The exposure time derived through the Beer-Lambert equation is then used as a starting point for initial dose experiments. In conjunction with the method described previously, an empirical approach can be used as well [24]. In chapter 2, a derivation for the resultant intensity was performed relating the individual intensities I_1, I_2, and an interference term I_{12}. If it is assumed that the two beams have equal intensities and are completely in phase, that is the interference term reduces to a value of 1, then the resultant intensity will yield a value of 4I. By utilizing this relation, an optimum exposure time can be empirically determined for a specific period, or angle of incidence, by conducting multiple exposures with only one beam for varying times (figure 3.9). Following development, the amount of photoresist removed can be measured using the ellipsometer and a correlation found between exposure times and post development resist thickness.

Once the desired thickness, due to exposure and development is found, the corresponding exposure time can be determined. This empirical quantification is predicated on the assumption that both beams are equal in intensity. If the condition holds true, then the exposure time that corresponds to the desire resist thickness will be divided by 4, since the resultant intensity is 4 times the individual.

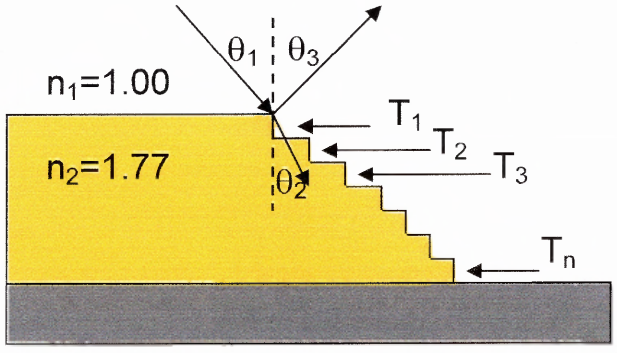

Figure 3.9 Procedure to empirically determine optimum exposure time.

The empirical quantification of an accurate exposure time was conducted by masking off the majority of the prepared substrate, except for a 25.4 mm aperture, and removing the dielectric mirror (Figure 3.10). This effectively removes one of the beams of the interferometer. The substrate was positioned for an incident angle of 30 degrees so that the visibility remained high across the complete area of exposure. The unmasked portion corresponds to the size of the mirror of the wavefront-division interferometer, which is the eventual area exposed to the desired fringe pattern. The exposed area of the masked wafer was illuminated for a specific exposure time, and then the wafer was rotated and exposed again for a different time. This procedure was repeated for a range of times from 7 to 21 minutes in duration. Upon completion the wafer was developed and the different exposures

were measured using the ellipsometer. The results (Figure 3.11) indicate that an exposure time of 21 minutes correspond to the removal of 500 nm of photoresist. This lead to an exposure time of roughly 5 minutes and 30 seconds and will be the starting point for future exposures.

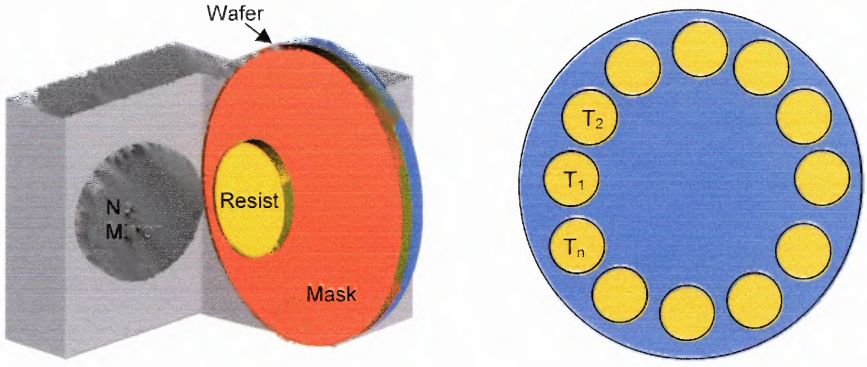

Figure 3.10 Configuration for empirical quantification of exposure time.

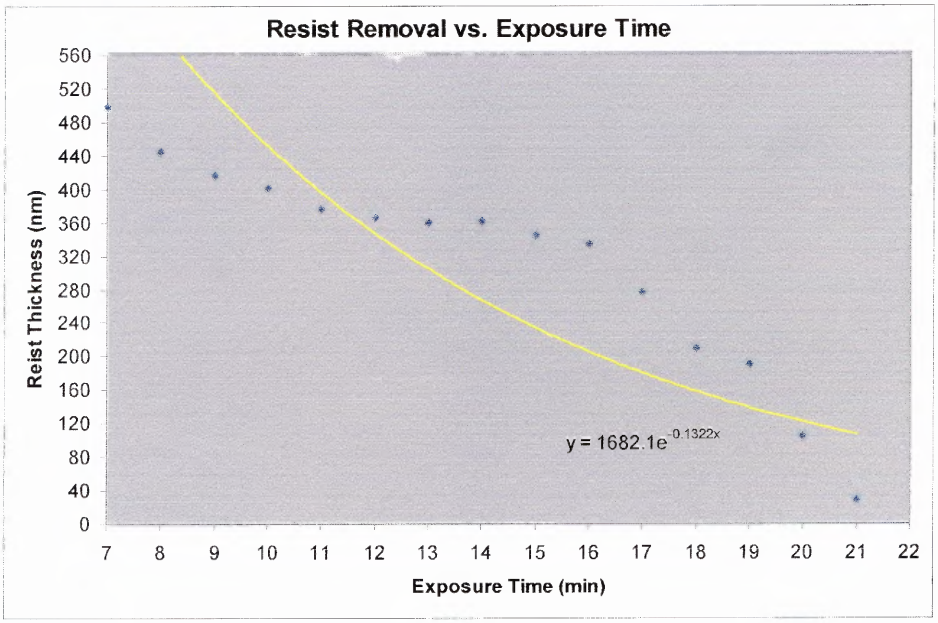

Figure 3.11 Resist removal versus exposure time.

3.3 Results and Discussion

The exposure time that was determined in the dose quantification was used as the starting point for full two beam interference exposures. The dielectric mirror was inserted back into the Lloyd's interferometer (figure 3.12), and the wafer with 500 nm resist was mounted.

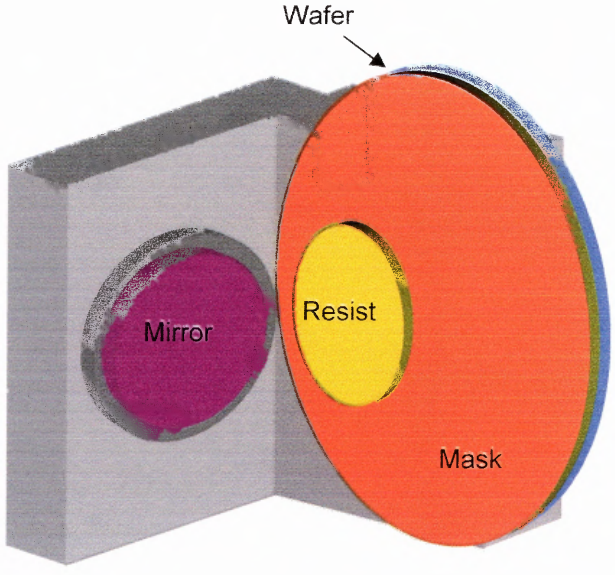

Figure 3.12 Lloyd's interferometer.

A "swing" curve of exposures was performed for incremental times, above and below the 5 minute 30 second exposure determined from the quantification experiment. It should be noted that any deviation of the incident angle will result in a difference in exposure time. The absorption and reflection of radiation by the photoresist is a function of incident angle and any dose quantification and future exposure must maintain the same angle. Different periods of resolution will have different exposure times and will require individual quantification.

Prior to inspection under the SEM, it is often advantageous to perform diagnostics on the integrity of the structure and exposure process [25], [26]. A technique was implemented to assess the quality of the grating structure. A Helium Neon, collimated

beam of radiation was traversed across the photoresist grating structure (figure 3.13). The exposed structure serves as a diffraction grating sending, a majority of the incident light into first and zero orders. A power meter was used to measure the power in each beam. A ratio between the first and zero order was calculated and referred to as grating "efficiency".

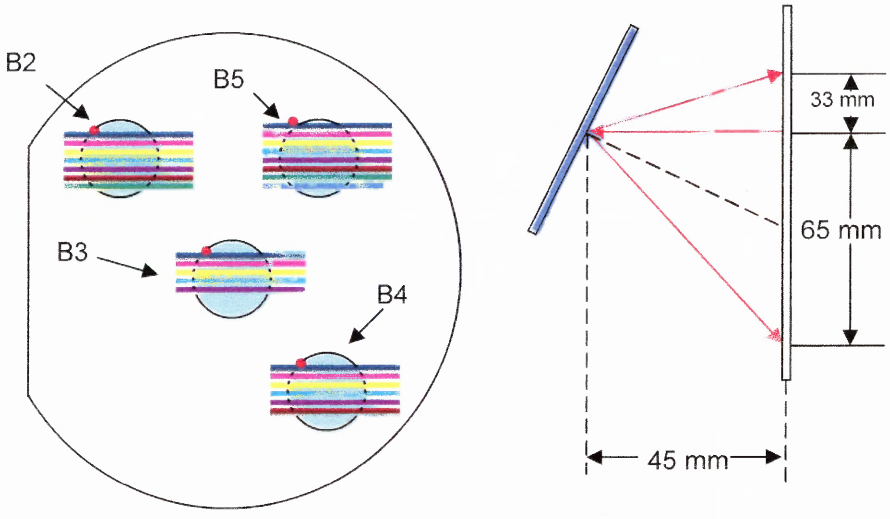

Figure 3.13 Grating efficiency measurement setup.

These scans were performed on all exposed areas in order to provide an initial feedback on the quality of the underlying structure. The efficiency measurements were performed by sampling multiple slices of the exposure in different vertical positions, while monitoring the power in each order. Exposures with sufficient grating efficiencies (Figure 3.14), were deemed acceptable for further investigation under the SEM. This technique serves as an effective way to discern the integrity of the grating structure before costly analysis in the SEM facility. A grating efficiency of at least 30% warranted further inspection under the electron microscope. Though no immediate quantitative information can be derived from grating efficiency, a strictly qualitative result can be determined. In theory, a structure with

high grating efficiency possesses a uniform structure with is suitable for further processing. Future research warrants determining a quantitative correlation between the grating efficiency and underlying grating structure.

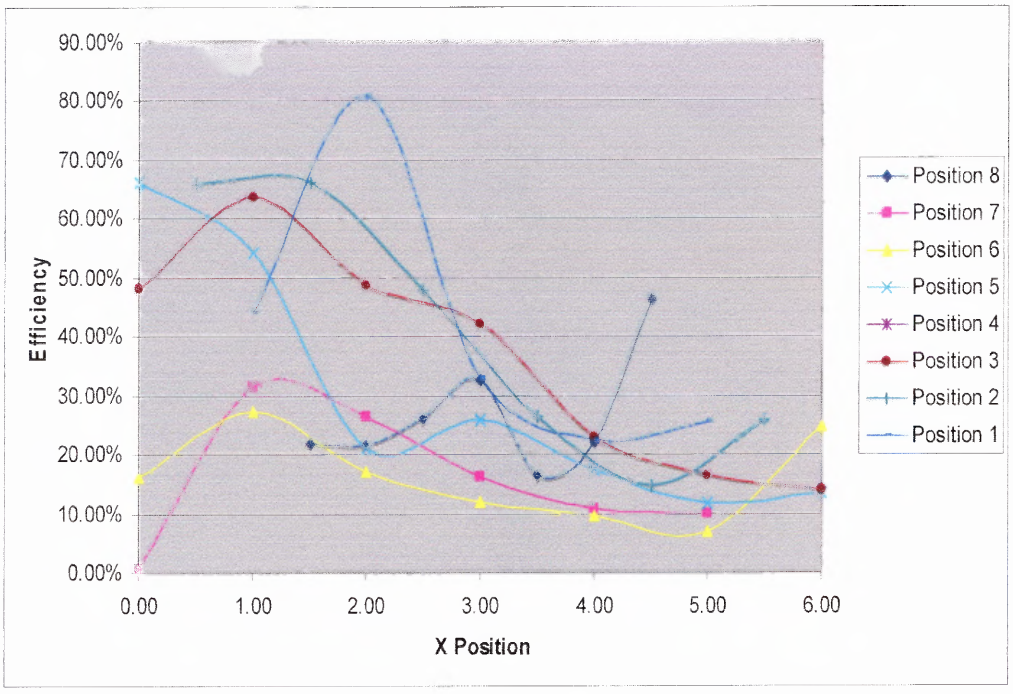

Figure 3.14 Grating efficiency measurements of acceptable structure.

The exposure samples deemed acceptable through the grating efficiency measurements were later inspected under the SEM. Results (Figures 3.15 and 3.16), indicate that a large area, high density, nanometer resolution grating structure was achieved. Upon closer inspection (Figure 3.17), it was also observed that the grating period achieved was roughly 585 nm. In addition, the structure appeared somewhat degraded with ragged edges and non–uniformities. These degradations could be the result of contamination during the post exposure process, and inconsistencies in the beam resulting in non uniformity during the exposure.

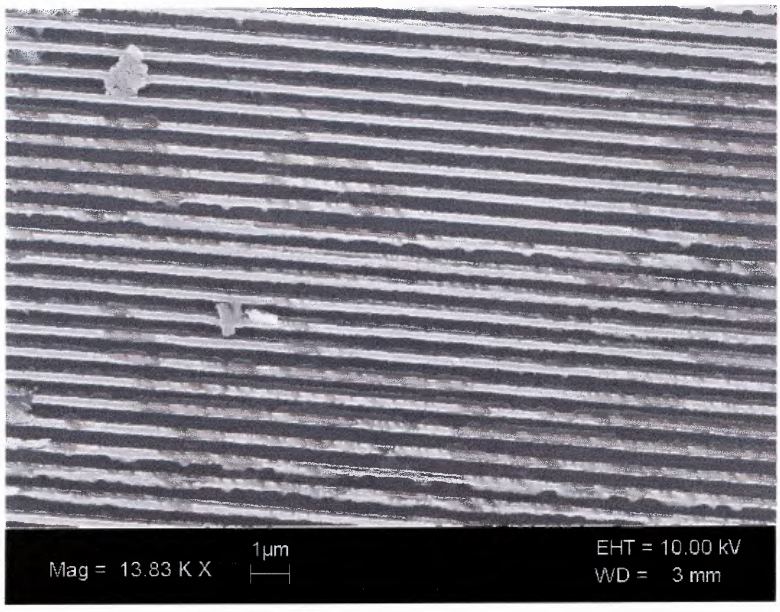

Figure 3.15 SEM image of large area grating structure.

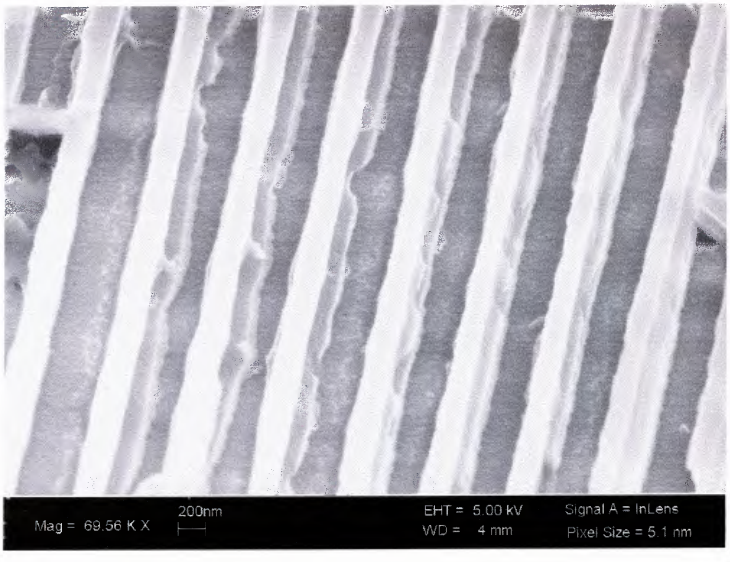

Figure 3.16 Enlarged SEM image of grating structure.

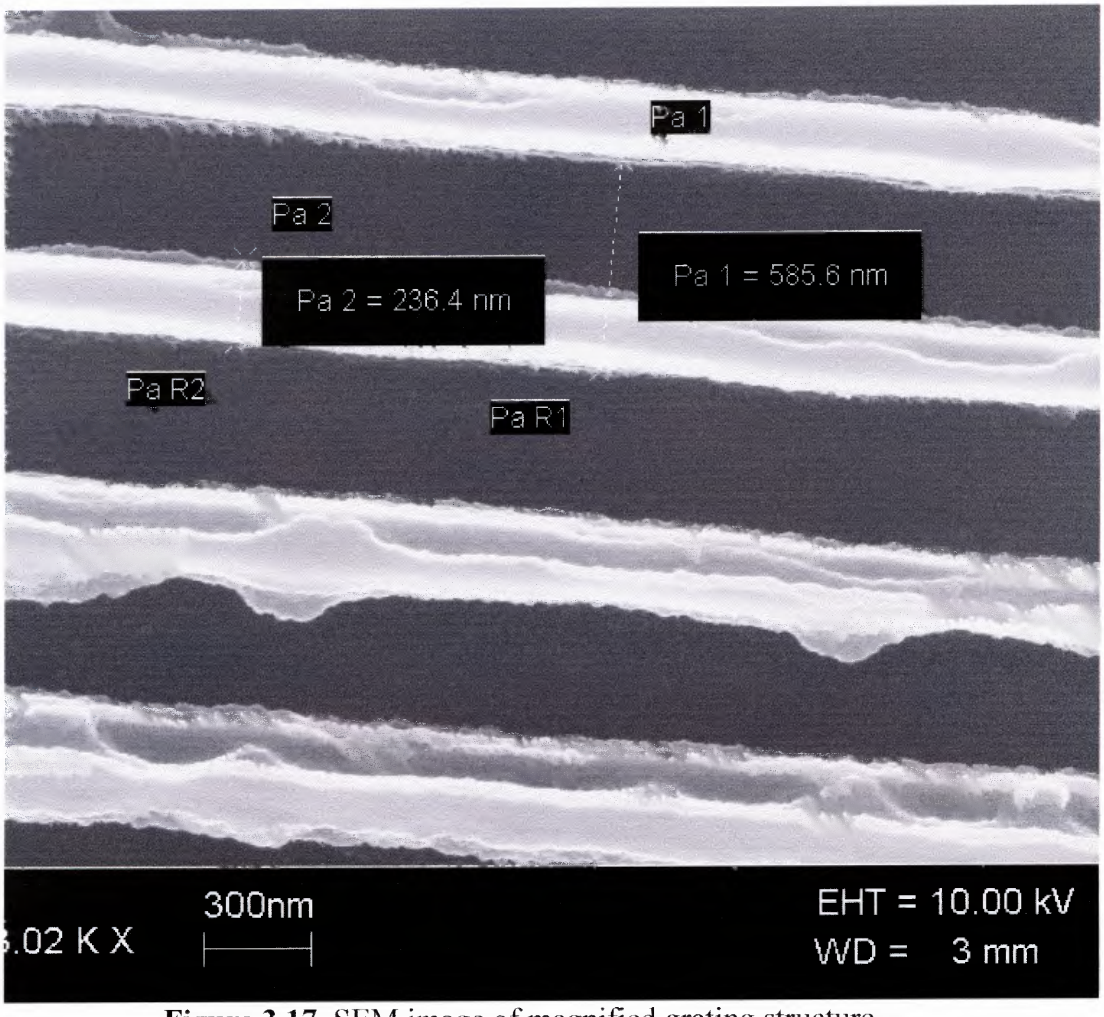

Figure 3.17 SEM image of magnified grating structure.

A profile, with horizontal (Figure 3.18) and vertical (Figure 3.19) dimensions, of the grating structure was obtained providing an illustration of the irregularities viewed previously. Immediately, two observations can be made. The grating structures were not uniformly exposed resulting in resist material remaining in between the linewidths. An ideal structure exhibits uniform sidewalls descending down to the wafer, facilitating ideal pattern transfer. The results indicate that the visibility may not be high enough due to an inequality in the intensity between the two beams in the interferometer. Most notable is the rippling effect present on the grating sidewalls. This is a ramification of an additional

interference that occurs between the incident beams at their reflections off the index of refraction mismatch leading to the formation of a standing wave which exposes the resist in the vertical direction.

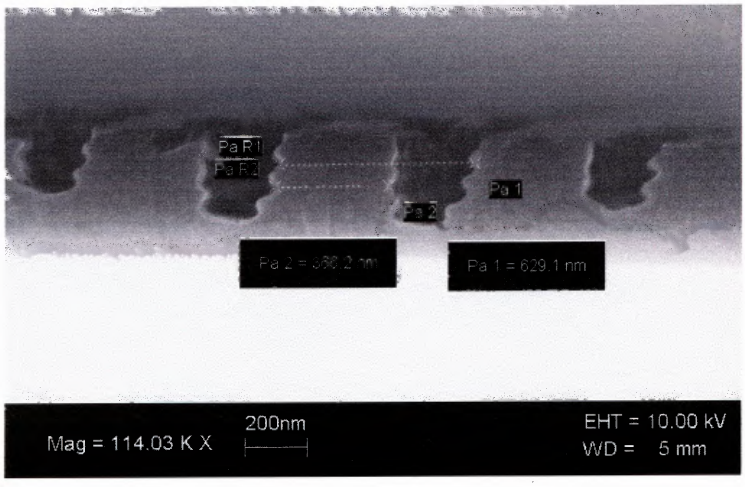

Figure 3.18 SEM image of profile of grating structure with horizontal dimensions.

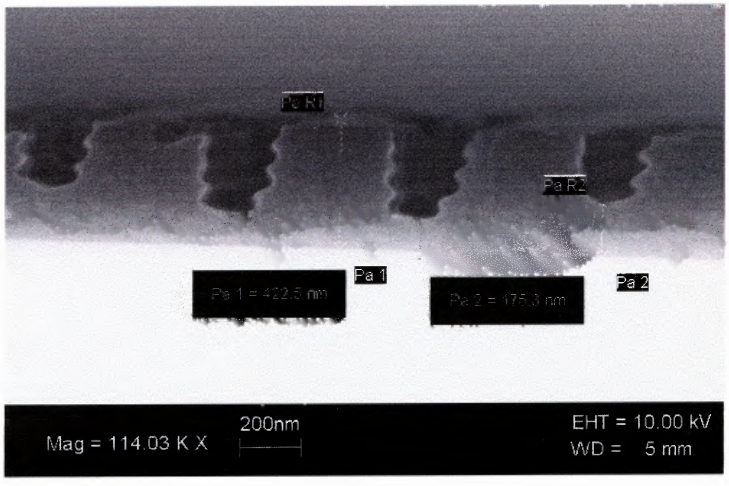

Figure 3.19 SEM image of profile of grating structure with vertical dimensions.

CHAPTER 4

CONCLUSION AND FUTURE WORK

In summary, this thesis presents the derivation, fabrication, and initial results of a nanopatterning technique called Interference Lithography. After several iterations that sought to enlist the attributes of an amplitude division interferometer, a wavefront division interferometer was employed to generate a fringe pattern with variable resolution capabilities. Utilizing a 325 nm HeCd laser, and conventional semiconductor wafer preparation techniques, optimum exposure conditions were determined through both conventional calculations and empirical assessment. Initial exposures yielded structure with sub 600 nm resolution, but suffered from structural imperfections. A cost effective, non-destructive, novel optical grating measurement was employed to provide a qualitative assessment of the integrity of the underlying structure. Upon sufficiently high grating efficiency the samples were later inspected under the SEM.

Despite the initial success and simplicity of the Lloyd's wavefront division interferometer, several limitations of the system warrant the eventual evolution to an amplitude division. The wavefront division interferometer will always be constrained by the geometry of the interferometer. Therefore, the area of exposure will be fixed to a small value depending on the coherence length of the source. However, even if the source has a sufficiently long coherence length the beam must be allowed to diverge over a great enough distance to ensure uniformity and plane wave approximation. This is a fairly significant drawback considering that the available power is considerably low due to the almost 50% loss from the spatial filter, and further decreases due to the gaussian beam

expansion. Perhaps, the largest drawback is the increase in exposure times. This is significant considering that the source has a finite lifetime, and longer exposure times will begin to have an adverse effect. In addition, prolonging the time that the wafer is exposed to environmental influences will undoubtedly lead to some form of non-uniformity that aberates the beam and is transferred to the final relief structure. Therefore, employing a higher powered source may be a logical option for obtaining nanostructures at reasonable exposure conditions.

The eventual transition to an amplitude division interferometer, Figure 4.1, justifies the added complexity and cost [27]. The primary benefit is that the beam divergences are minimized, ensuring that a majority of the intensity illuminates the wafer during exposure. In addition, the sample can be scanned over a large area allowing larger substrates to be used. Though the system employs additional components and computer control systems [28], the system utilizes the most crucial element for lithography, the source.

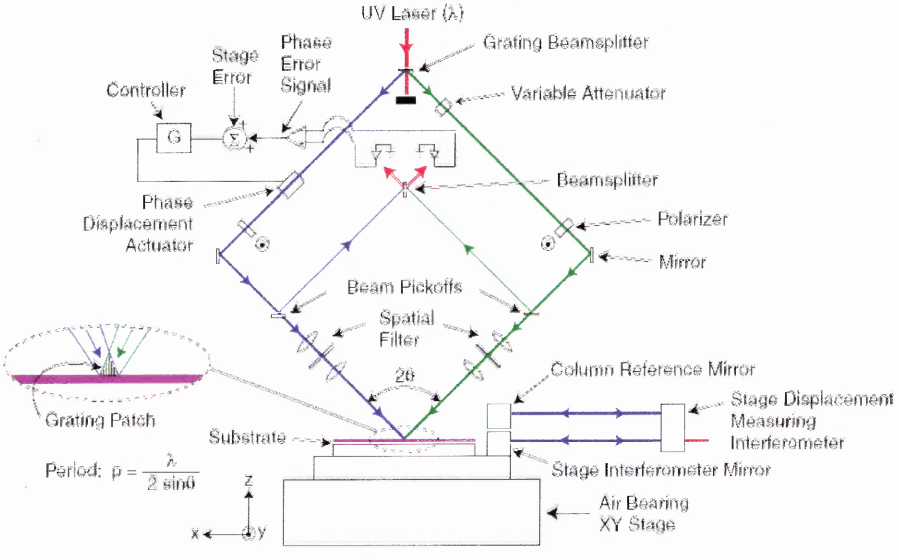

Figure 4.1 Amplitude division interferometer employed for scanning beam interference lithography [27].

The experimental results obtained, Figure 4.2, indicate the presence of vertical standing waves resulting from an additional interference that occurs between the incident beam and a reflected portion of itself from the highly reflective substrate interface, Figure 4.3. These additional interference fringes effectively expose the structure to a periodic pattern in the direction normal to the desired period. The standing wave interference exposes the base and sidewalls of the desired periodic pattern. The "rippling" effect is most evident in the SEM image and can lead to further deleterious effects, and may eventually result in the shearing off of the complete resist structure.

Figure 4.2 SEM image of vertical standing wave causing additional exposure.

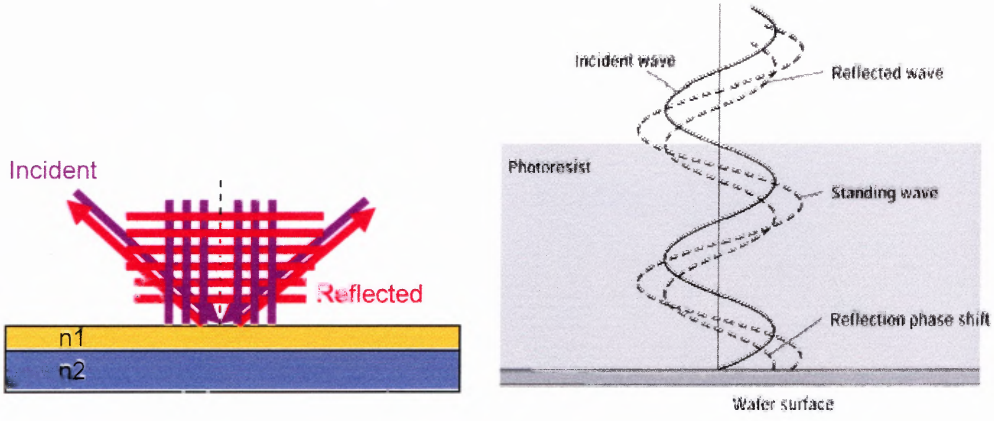

Figure 4.3 Diagram of standing wave and schematic of resulting interference.

To combat the deleterious effects induced by the vertical standing wave during exposure, research indicates that the addition of a thin interlayer, Figure 4.4, in conjunction with an anti reflection coating can successfully suppress the magnitude of the standing wave[29]. Traditionally, anti reflective coatings (ARC) induce a phase shift that effectively moves the maximum of the wave intensity to a position above the resist layer. Future exposures may potentially benefit from the inclusion of such a layer during the wafer preparation process.

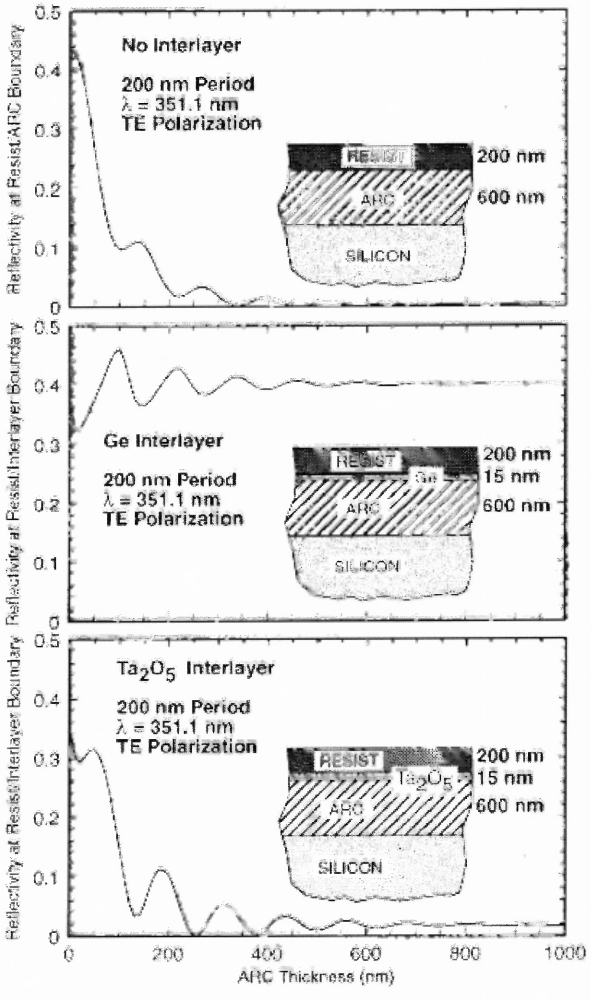

Figure 4.4 Reflectivity simulation of anti-reflective coating and interlayer [29].

Interference lithography can be extrapolated to include more than two beams [30]. By employing a multi beam configuration, Figure 4.5, the interference pattern generated can be used to generate three dimensional structures over a large area, Figure 4.6. By manipulating the relative amplitude, polarization, and phase of each beam the overall contrast of the interference pattern can be controlled and different lattice structures written. Such a technique opens the door for large scale, three dimensional photonic bandgap structures and templates for induced growth.

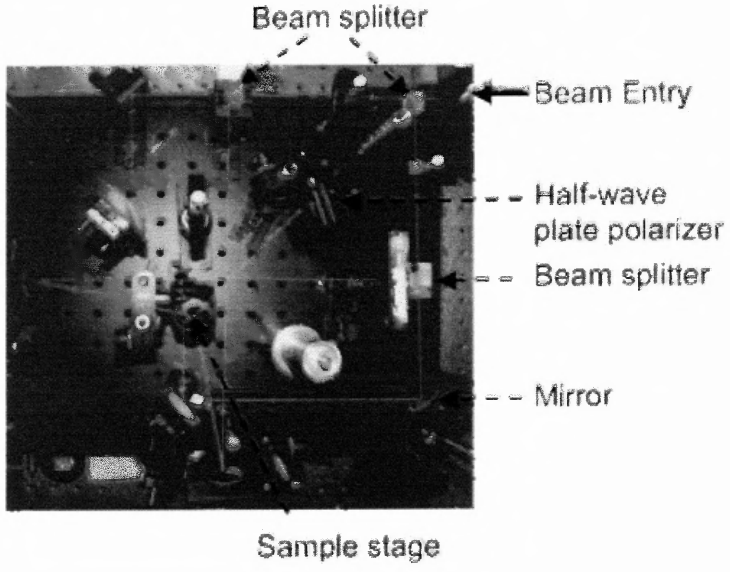

Figure 4.5 Multi-beam configuration for interference lithography [30].

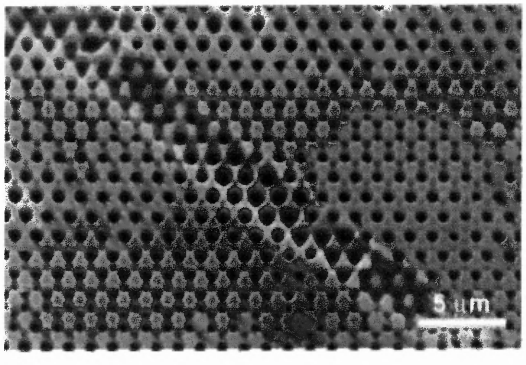

Figure 4.6 SEM image of three dimensional polymer microstructure [30].

One potential application of a successful exposure protocol is the induced growth and integration of semiconductor nanocrystals. Researchers have succeeded in the fabrication of silicon nanocrystals on a periodic template by using interferometric lithography [31]. The resultant grating pattern was transferred to the protective silicon oxide layer, grown on a silicon wafer, using reactive ion etching. Subsequent potassium hydroxide (KOH) anisotropic etching was performed resulting in nearly atomically smooth, inverted pyramid structures, Figure 4.7. These sub 50 nm dimension structures served as a template for demarcation, and induced growth of nanocrystal entities. These individually addressable nanocrystals hold promise for future device architectures.

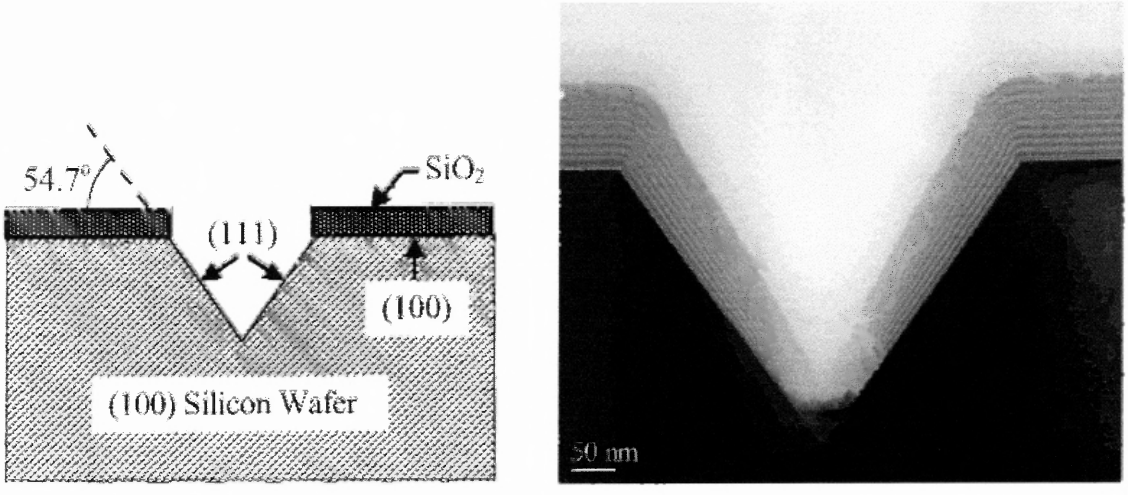

Figure 4.7 Selective etching of silicon wafer and subsequent growth of nanoclusters [31].

In conclusion, Interference Lithography is a straight forward, simplistic technique for patterning in the nanoscale regime. As conventional photolithographic systems continue to evolve in the push for smaller critical dimensions, interference lithography offers a complementary approach to utilizing existing fabrication protocols with out investing in cost prohibitive advanced stepper systems.

REFERENCES

1. International Technology Roadmap for Semiconductors (ITRS) Update. Retrieved May 25, 2006, from http://www.itrs.net/Links/2005ITRS/ExecSum2005.pdf

2. J. P. Silverman, "Challenges and progress in x-ray lithography." J. Vac. Sci. Technol. B 16, (1998) 3137.

3. C. W. Gwyn, R. Stulen, D. Sweeney, and D. Attwood, "Extreme ultraviolet lithography." J. Vac. Sci. Technol. B 16, (1998) 3142.

4. S. T. Stanton, J. A. Liddle, W. K. Waskiewicz, and A. E. Novembre, "Critical dimension control at stitched subfield boundaries in a high-throughput SCALPEL system." J. Vac. Sci. Technol. B 16, (1998) 3197.

5. G. Gross, R. Kaesmaier, H. Loschner, and G. Stengl, "Ion projection lithography: status of the MEDEA project and United States/European cooperation." J. Vac. Sci. Technol. B 16, (1998) 3150.

6. G. M. Whitesides and B. Grzybowski, "Self-assembly at all scales." Science v. 295, (2002) 2418.

7. N. Bowden, A. Terfort, J. Carbeck, and G. M. Whitesides, "Self-assembly of mesoscale objects into ordered two-dimensional arrays." Science v. 276, (1997) 233.

8. G. M. Whitesides and M. Boncheva, "Beyond molecules: self-assembly of mesoscopic and macroscopic components." PNAS v. 99. (2002) 4769-4774.

9. J. P. Spallas, A. M. Hawryluk, and D. R. Kania, "Field emitter array mask patterning using laser interference lithography." J. Vac. Sci. Technol. B 13, (1995) 1973.

10. M. J. O Brien, P. Bisong, L. K. Ista, E. M. Rabinovitch, A. L. Garcia, S. S. Sibbett, G. P. Lopez and S. R. J. Brueck, "Fabrication of an integrated nanofluidic chip using interferometric lithography." J. Vac. Sci. Technol. B 21, (2003) 2941.

11. Sang Ouk Kim, Harun H. Solak, Mark P. Stoykovich, Nicola J. Ferrier, Juan J. de Pablo and Paul F. Nealey, "Epitaxial self-assembly of block copolymers on lithographically defined nanopatterned substrates." Nature 424, (2003) 411.

12. X. Li, A. Cao, Y. J. Jung, R. Vajtai, and P. M. Ajayan, "Bottom-up growth of carbon nanotube multilayers: unprecedented growth." Nano Letters 5(10), (2005) 1997.

13. M. Rothschild, T. M. Bloomstein, N. Efremow, T. H. Fedynyshyn, M. Fritze, I. Pottebaum, M. Switkes, "Nanopatterning with UV optical lithography." MRS BULLETIN 30(12), (2005) 942.

14. M. Switkes, M. Rothschild, R. R. Kunz, S-Y. Baek, D. Coles and M. Yeung, "Immersion lithography: Beyond the 65nm node with optics." Microlithography World, 4, May (2003).

15. J. Y. Decker, A. Fernandez, and D. W. Sweeney, "Generation of subquarter-micron resist structures using optical interference lithography and image reversal." J. Vac. Sci. Technol. B 15, (1997) 1949.

16. A. Fernandez, J. Y. Decker, S. M. Herman, D. W. Phillion, D. W. Sweeney, and M. D. Perry, "Methods for fabricating arrays of holes using interference lithography." J. Vac. Sci. Technol. B 15, (1997) 2439.

17. S. Zaidi, and S. Brueck, "High aspect-ratio holographic photoresist gratings." Appl. Opt. 27(14), (1988) 2999.

18. L. F. Johnson, G. W. Kammlott, and K. A. Ingersoll, "Generation of periodic surface corrugations." Appl. Opt. 17(8), (1978) 1165.

19. B. Mello, I. Costa, C. Lima, and L. Cescato, "Developed profile of holographically exposed photoresist gratings." Appl. Opt. 34(4), (1995) 597.

20. G. Schmid, M. Stewart, S Burns, and C. G. Willson, "Mesoscale monte carlo simulation of photoresist processing." J. Electrochemical Soc. 151 (2), (2004).

21. J. Shin, G. Han, Y. Ma, K. Moloni, and F. Cerrina, "Resist line edge roughness and aerial image contrast." J. Vac. Sci. Technol. B 19, (2001) 2890.

22. A. Pawloski, A. Acheta, I. Lalovic, B. La Fontaine, and H. Levinson, "Characterization of line edge roughness in photoresist using an image fading technique." SPIE Vol. 5376, (2004) 414.

23. W. Hinsberg, F. A. Houle, J. Hoffnagle, M. Sanchez, G. Wallraff, M. Morrison, and S. Frank, "Deep-ultraviolet interferometric lithography as a tool for assessment of chemically amplified photoresist performance." J. Vac. Sci. Technol. B 16, (1998) 3689.

24. S. Austin, and F. T. Stone, "Fabrication of thin periodic structures in photoresist: a model." Appl. Opt. 15(4), (1976) 1071.

25. M. S. Sthel, C. Lima, and L. Cescato, "Photoresist resolution measurement during the exposure process." Appl. Opt. 30(35), (1991) 5152.

26. S. Sohail, H. Naqvi, S. Zaidi, S. Brueck, and J. McNeil, "Diffractive techniques for lithographic process monitoring and control." J. Vac. Sci. Technol. B 12, (1994) 3600.

27. C. G. Chen, P. T. Konkola, R. K. Heilmann, C. Joo and M. L. Schattenburg, "Nanometer-accurate grating fabrication with scanning beam interference lithography." SPIE Vol. 4936, (2003) 126.

28. R. K. Heilmann, P. T. Konkola, C. G. Chen, G. S. Pati, and M. L. Schattenburg, "Digital heterodyne interference fringe control system." J. Vac. Sci. Technol. B 19, (2001) 2342.

29. M. L. Schattenburg, R. J. Aucoin, and R. C. Fleming, "Optically matched trilevel resist process for nanostructure fabrication." J. Vac. Sci. Technol. B 13, (1995) 3007.

30. J. H. Moon, J. Ford, and S. Yang, "Fabricating three-dimensional polymeric photonic structures by multi-beam interference lithography." Polym. Adv. Technol. 17, (2006) 83.

31. C. Striemer, R Krishnan, P. M. Fauchet, and L. Tsybeskov, "Controlled nucleation of silicon nanocrystal on a periodic template." Nano Lett. 1(11), (2001) 643.